1984

The effect of prior parent phase cold work on martensite transformation in Cu-An-Al shape memory alloys.

Moore, Gary E.

NAVAL POSTGRADUATE SCHOOL

Monterey, California

THESIS

THE EFFECT OF PRIOR PARENT PHASE COLD WORK ON MARTENSITE TRANSFORMATION IN Cu-Zn-Al SHAPE MEMORY ALLOYS

by

Gary E. Moore

December 1984

Thesis Advisor: J. Perkins

Approved for public release; distribution unlimited

SECURITY CLASSIFICATION OF THIS PAGE *(When Data Entered)*

REPORT DOCUMENTATION PAGE		READ INSTRUCTIONS BEFORE COMPLETING FORM
1. REPORT NUMBER	2. GOVT ACCESSION NO.	3. RECIPIENT'S CATALOG NUMBER
4. TITLE *(and Subtitle)* The Effect of Prior Parent Phase Cold Work on Martensite Transformation in Cu-An-Al Shape Memory Alloys		5. TYPE OF REPORT & PERIOD COVERED Master's Thesis; December 1984 6. PERFORMING ORG. REPORT NUMBER
7. AUTHOR(s) Gary E. Moore		8. CONTRACT OR GRANT NUMBER(s)
9. PERFORMING ORGANIZATION NAME AND ADDRESS Naval Postgraduate School Monterey, California 93943		10. PROGRAM ELEMENT, PROJECT, TASK AREA & WORK UNIT NUMBERS
11. CONTROLLING OFFICE NAME AND ADDRESS Naval Postgraduate School Monterey, California 93943		12. REPORT DATE December 1984 13. NUMBER OF PAGES 84
14. MONITORING AGENCY NAME & ADDRESS*(if different from Controlling Office)*		15. SECURITY CLASS. *(of this report)* Unclassified 15a. DECLASSIFICATION/DOWNGRADING SCHEDULE

16. DISTRIBUTION STATEMENT *(of this Report)*

Approved for public release; distribution unlimited

17. DISTRIBUTION STATEMENT *(of the abstract entered in Block 20, if different from Report)*

18. SUPPLEMENTARY NOTES

19. KEY WORDS *(Continue on reverse side if necessary and identify by block number)*

Shape Memory Effect
Martensitic Transformation
Copper Base Alloys
Cu-Zn-Al
Cold Work

20. ABSTRACT *(Continue on reverse side if necessary and identify by block number)*

The effect of cold work upon the transformation kinetics of parent to martensite and martensite to parent was studied utilizing differential scanning calorimetry, x-ray diffraction, optical and transmission electron microscopy methods. Samples of a Cu-Zn-Al shape memory alloy were cold rolled above M_s (martensite start temperature) to varying degrees of deformation. The cold work samples displayed various deformation morphologies.

DD FORM 1 JAN 73 1473 EDITION OF 1 NOV 65 IS OBSOLETE

S/N 0102-LF-014-6601

SECURITY CLASSIFICATION OF THIS PAGE *(When Data Entered)*

20. (Continued)

The mechanisms by which these deformation morphologies were developed and the varying morphology crystallographic features were studied and characterized using x-ray diffraction and optical and transmission electron microscopy techniques.

The Effect of Prior Parent Phase Cold Work on Martensite Transformation in Cu-Zn-Al Shape Memory Alloys

by

Gary E. Moore
Lieutenant Commander, United States Navy
B.S., Indiana University, 1973

Submitted in partial fulfillment of the
requirements for the degree of

MASTER OF SCIENCE IN MECHANICAL ENGINEERING

from the

NAVAL POSTGRADUATE SCHOOL
December 1984

ABSTRACT

The effect of cold work upon the transformation kinetics of parent to martensite and martensite to parent was studied utilizing differential scanning calorimetry, x-ray diffraction, optical and transmission electron microscopy methods. Samples of a Cu-Zn-Al shape memory alloy were cold rolled above M_s (martensite start temperature) to varying degrees of deformation. The cold worked samples displayed various deformation morphologies. The mechanisms by which these deformation morphologies were developed and the varying morphology crystallographic features were studied and characterized using x-ray diffraction and optical and transmission electron microscopy techniques.

TABLE OF CONTENTS

LIST OF TABLES

LIST OF FIGURES

LIST OF MICROGRAPHS

ACKNOWLEDGEMENT

This research was sponsored by the National Science Foundation Research Program: "Martensitic Transformations in Shape Memory Alloys."

Thanks are due to Professor Jeff Perkins for initial program formulation and guidance, Tom Kellogg and Dr. Prabir Deb for technical assistance and to Captain Garritson, Captain Johnson, and Commander Ericson, prior and current Naval Engineering Curricular Officers, for their support and encouragement.

Special thanks is due to Dr. Kenji Adachi who provided expert instruction and guidance in optical and TEM microscopy and interpretation of experimental data.

Finally, I want to thank those who provided the most support, encouragement and many prayers, my wife, Yvonne, and children, Tegan, Garett, and Galen.

I. INTRODUCTION

Shape memory effect (SME) is the property of certain alloys to sustain deformation which appears to be permanent, but then, upon unloading or thermal treatment, the alloy reverts back to its original shape. This process is illustrated in Figure 1 [Ref. 1]. Shape memory effect phenomena is directly related to thermoelastic martensitic transformations. Shewmon [Ref. 2] categorizes general martensitic transformation characteristics as follows: 1) tranformation is accomplished by shearing and the martensitic plates lie along a habit plane; 2) the transformation is diffusionless; 3) the martensite-matrix interface is glissile and consists of arrays of dislocations; 4) martensite starts forming at a particular temperature M_s (martensite start temperature) and stops forming martensite at a lower particular temperature M_f (martensite finish temperature); 5) plastic deformation below the M_s will increase the amount of martensite and deformation at temperatures up to the martensite deformation temperature (M_d) will cause martensite to nucleate; and 6) the low-temperature phase formed martensitically on cooling will revert to the high-temperature phase on heating above the A_s (parent phase start temperature) as long as

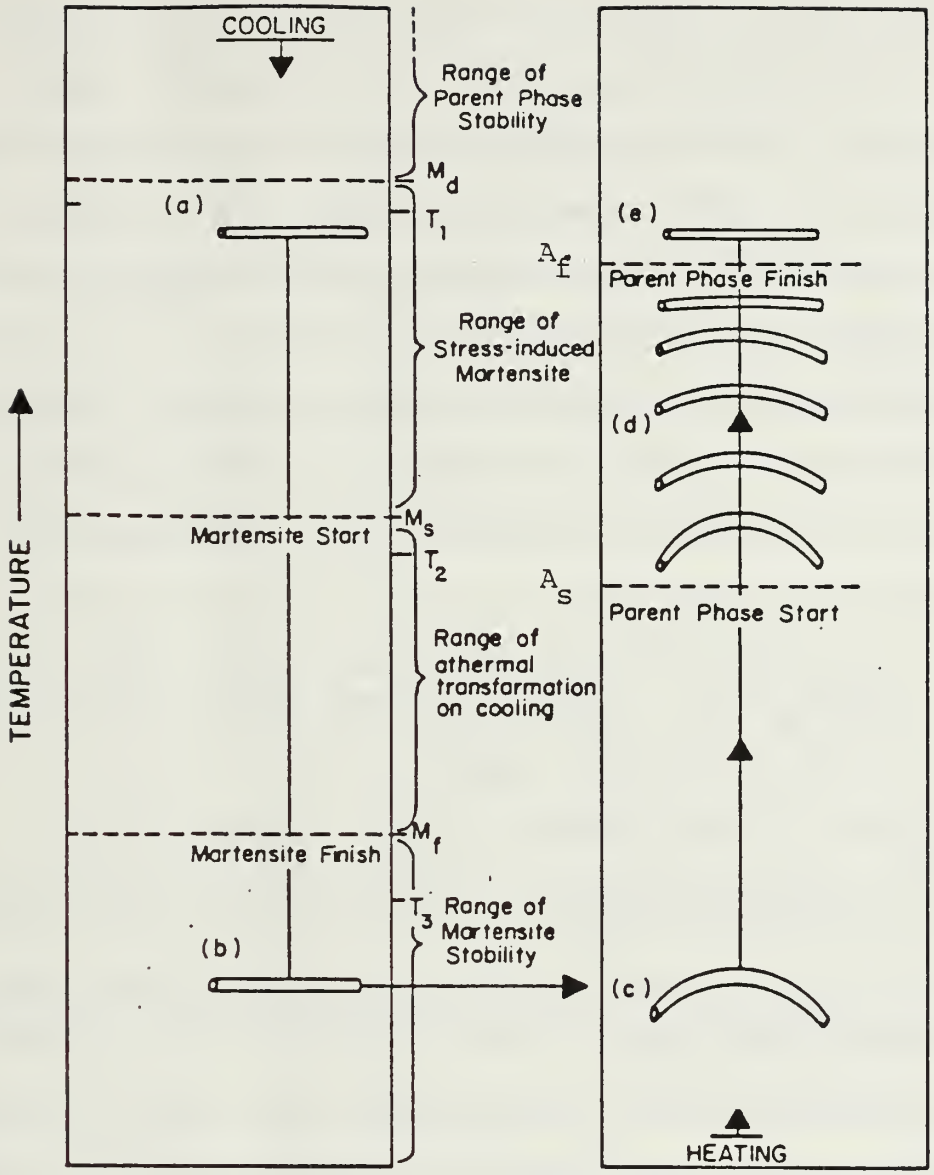

Figure 1. Schematic Description of the Shape Memory Effect (SME): (a) straight parent phase wire; (b) cooled through the athermal transformation range M_s to M_f produces a straight martensite wire; (c) deformed martensite wire; (d) straightens out when heated through reverse transformation range A_s to A_f, reproducing the straight parent phase wire. Note that there is typically a slight hysteresis between the forward and reverse transformation ranges, so that the transformation on cooling, P -> M, occurs over a slightly lower range (M_s to M_f) than the transformation on heating, M -> P (A_s to A_f). M_d is the temperature below which martensite can be stress-induced from the parent phase.

precipitation reaction has not taken place in the low-temperature phase. Nishiyama [Ref. 3] further defines martensitic transformation as a phase transformation due to cooperative atomic movements including the additional characteristics of surface relief and the presence of many lattice imperfections.

Thermoelastic martensite transformations, a property of shape memory alloys, can be characterized by the presiding generalized properties of martensitic transformations with the following properties outlined by Nishiyama [Ref. 3]:

1) Thermoelastic martensite plate growth and shrinkage, occurs under a balance between thermal and elastic effects (i.e., the chemical driving force is balanced by the nonchemical energy),

2) Small lattice deformation for transformation,

3) Martensites containing internal twins which can easily be detwinned, and

4) Martensites must have an ordered structure that cannot be destroyed by slip during thermoelastic martensitic transformations.

As the temperature is lowered and/or the stress is increased martensite forms continuously and shrinks along the same path as the temperature is increased and/or the stress is decreased. Thermoelastic behavior should have low hysteresis and no plastic deformation, on the reversal of temperature [Ref. 4]. However, there is increasing evidence that, at least on initial transformation cycles, this is not the case on a microscopic scale, and that local dislocation production occurs [Ref. 5].

Thermoelastic behavior has been observed in many binary and ternary noble-metal-base alloys. This study has concentrated on such an alloy, namely a Cu-Zn-Al beta phase alloy. The Cu-Zn-Al beta phase alloys exist in the parent phase as an ordered body centered cubic (BCC) crystal structure and transform thermoelastically to a close packed layered martensitic structure having a long-period stacking order based on prior {110} planes of the parent phase. The parent to martensitic transformation reaction is

$$B2\ (DO_3) \rightarrow 3R\ (6R),\ 9R\ (18R),\ 2H$$

where the martensite (beta prime) phase, 3R (6R), 9R (18R), or 2H, has a stacking sequence of ABC (AB´CA´BC´), ABCBCACAB (AB´CB´CA´CA´BA´BC´BC´AC´AB´), OR AB (AB´) [Ref. 6].

Shape memory alloys are being utilized more frequently in industrial and commercial applications and as their potential is realized will become an important class of alloys. The ternary Cu-Zn-Al shape memory alloys are of particular interest because of the many advantages in their relatively low cost and ease of fabrication. This alloy system also offers a wide range of martensite transformation temperatures produced by varying alloy concentrations.

The purpose of this study was to determine the effect of cold work upon the transformation kinetics of parent to

martensite and martensite to parent during transformation cycling of a particular Cu-Zn-Al shape memory alloy.

II. EXPERIMENTAL PROCEDURE

A. SAMPLE PREPARATION

The alloys examined were supplied by Delta Metals Research Limited, Ipswich, Suffolk, England. The primary samples used in this research are designated as alloy D with a composition of 66.2 atomic percent Cu, 24.8 atomic percent Zn, and 9 atomic percent Al. Alloy B with a composition of 69.3 atomic percent Cu, 14.6 atomic percent Zn, and 16.1 atomic percent Al and alloy C with a composition of 68.0 atomic percent Cu, 18.9 atomic percent Zn, and 13 atomic percent Al was used for comparison. The alloys were received as bars with a diameter of 1.27 cm. A 7 cm long square bar sample was machined from the round stock with a diagonal approximately 1 cm. The sample was sealed in an evacuated quartz tube, homogenized for 20 minutes at 850^{o}C and quenched in ice water. Seven cubes one cm on a side were then cut from the sample bar using a low speed diamond saw. Each sample cube was then cold rolled to varying degrees of deformation using a Fenn laboratory rolling mill (5 HP and 10.5 cm diameter rollers). The sample cubes were cold rolled at room temperature decreasing the roller bite increment approximately 0.10 mm each run through the mill. The average percent of cold work H was defined as:

$$H = \frac{H_o - H_f}{H_o} \times 100$$

H_o = original height of bar prior to rolling

H_f = final height of bar after rolling

Table I lists the various degrees of deformation. The maximum deformation achieved was 22.4 percent. At 22.4 percent, cracking was just starting to appear on the sample surfaces parallel to the direction of force.

TABLE I

SAMPLE IDENTIFICATION AND PERCENT COLD WORK

Sample Number	Cold Work (%)
1	0.00
2	2.2
3	5.1
4	6.5
5	13.9
6	18.6
7	22.4

B. OPTICAL MICROSCOPY

All sample cubes were cut transverse and parallel to the longitudinal axis of the direction of rolling to provide specimens for optical microscopy. All cuts were made with a

low speed diamond saw and the specimens were cut away from the ends of the bars to avoid anomalies due to end effects. Each specimen was polished by the following procedure:

1) Sand on 320 grit emery paper.
2) Sand on 400 grit emery paper.
3) Sand on 600 grit emery paper.
4) Electropolish for 30 seconds at 10 volts and for 30 seconds at 8 volts in a solution of phosphoric acid (H_3PO_4) saturated with cromic acid (CrO_3) with a standard steel anode.

Photomicrographs were taken with Kodak technical pan film 2415 using a Zeiss photomicroscope.

C. DIFFERENTIAL SCANNING CALORIMETRY

Discs, 3.0 mm in diameter were punched with a TEM 3.0 mm sample punch from thin plates approximately 0.25 mm thick cut from the sample cubes. Each disc was prepared essentially the same as the optical microscopy samples. All sample weights were within $\pm$10% of the 0.00 percent cold work (standard) sample which was .0138 gms as weighed on a sartorius balance. The differential scanning calorimeter (DSC) analysis provided experimental data on the thermal properties of the parent to martensite and martensite to parent transformations. The DSC used was a Perkin-Elmer (DSC-2). The DSC measures the power required to maintain a sample and holder at the same temperature as a reference holder as the reference holder is cycled thermally through a

programmed heating and cooling routine. The transition from parent to a martensite phase is exothermic while transition from martensite to parent is endothermic. The DSC profile of a tranformation process is illustrated schematically by Figure 2 [Ref. 7]. The kinetic parameters measured for alloys B, C, and D were:

M_s Martensite start temperature;

M_f Martensite finish temperature;

M_{max} Peak temperature for the forward transformation;

A_s Parent start temperature;

A_f Parent finish temperature;

A_{max} Peak temperature for the reverse transformation;

A_{max} and M_{max} are defined as the temperature at which the maximum transformation rate occurred. A_s, A_f, M_s, and M_f are determined as the departure point from the baseline curve. This value was pinpointed by constructing a near tangent line to the transformation curves and the point where the tangent line intersected the pre/post-transformation baselines was recorded as the A_s, A_f, M_s, and M_f parameters. Difficulty maintaining a DSC steady cooling rate below approximately 235 Kelvin and obtaining an initial zero baseline slope subjects alloy D data to some interpretation, but relative peak shape and area and maximum peak temperatures are accurate enough to form sound experimental judgements.

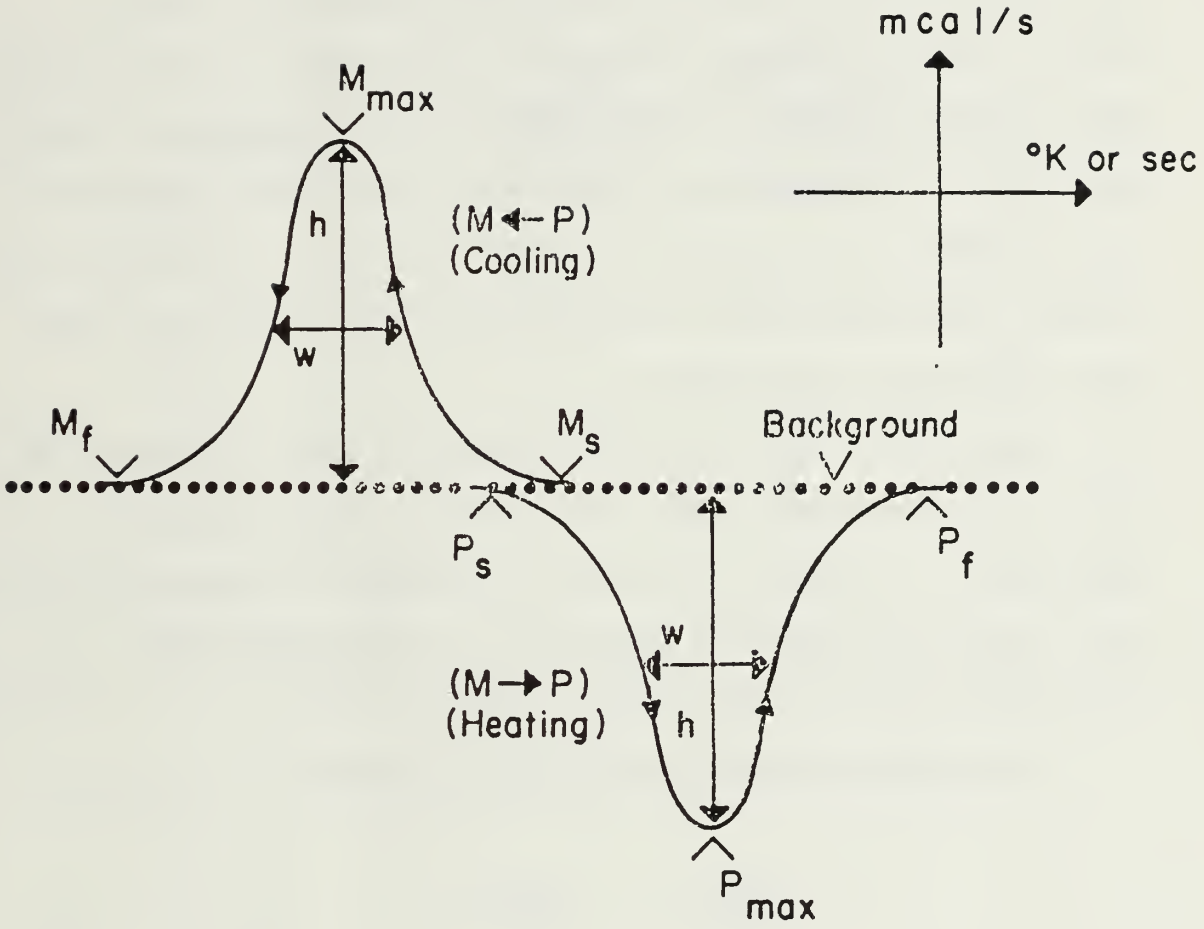

Figure 2. Schematic Differential Scanning Calorimeter Profiles for P -> M and M -> P Transformations, Defining the Kinetic Parameters, Including the Transformation Temperatures (M_s, M_f, M_{max}, A_s, A_f, A_{max}) and the Peak Height and Peak Width at 1/2-Height

D. X-RAY DIFFRACTION ANALYSIS

X-ray diffraction bulk samples were cut from the sample cubes using a low speed diamond saw. and mounted in a standard sample holder. The powder sample was made by filing the 0.0 percent cold work bulk sample. The filings were sifted through a U.S. standard sieve series to obtain powder particles smaller than 88 microns. The powder was then sealed in an evacuated quartz tube and back filled with argon. The powder was homogenized for 15 minutes at 850°C and quenched in ice water.

The powder sample was then analyzed with a Philips XRG 3100 x-ray generator and Norelco data control processor. A sequence of heavier and heavier cold work was then performed on the powder sample by hammering and the sample was reanalyzed after each increment of cold work.

The Nelson-Riley extrapolation function:

$$\frac{\cos^2\theta}{\sin\theta} + \frac{\cos^2\theta}{\theta}$$

was used to determine the lattice parameters of the parent beta phase and the precipitated alpha phase. Table II identifies the sample runs and lists the equipment settings.

E. TRANSMISSION ELECTRON MICROSCOPY (TEM)

Only preliminary TEM work has been completed. As received alloy D stock was quartered and machined into 3 mm

TABLE II

X-RAY DIFFRACTION SAMPLE IDENTIFICATION AND EQUIPMENT SETTINGS (ALLOY D)

Run	% Coldwork	Time Constant (sec)	Scanning Rate (Deg/min)	KV	mA
1	0.0	1	1°	35	10
2	5.1	1	1°	40	20
3	6.5	1	1°	40	20
4	22.4	1	1°	40	20
5	0.0 (Powder)	1	1°	30	15
6	Light (Powder)	1	1°	45	25
7	Moderate (Powder)	1	1°	40	25
8	Heavy (Powder)	1	1°	40	25

(Multiplier = 2 with exception of Run 8 which was 1)

diameter bars. The bars were sealed in evacuated quartz tubes and homogenized for 20 minutes at 900°C and quenched in ice water. The samples were then cold worked by extruding with a swaging machine. The samples were then cut with a slow speed diamond saw to approximately 0.2 mm thick TEM specimens. The specimens were jet polished with a streuers polipower rectifier and tenupol unit using 3% perchloric acid/methanol solution. The TEM foils were then examined and photographed with Kodak electron microscope film 4489 using a JEM-100 CX II, electron microscope.

III. RESULTS AND DISCUSSION

A. DIFFERENTIAL SCANNING CALORIMETRY

Initial differential runs of 100 cycles each for samples of alloy B and D were run to develop DSC profiles and to determine at what point the alloys' thermal characteristics become stable. Previous work [Ref. 7] have reported that both exothermal and endothermal transformation temperatures and the peak profiles change as the alloys are cycled between two temperatures covering the whole range of characteristic transformation temperatures. Some unexpected results were obtained and are presented in the following figures. Figures 3 through 6 are the peak maximum on DSC profiles, M_{max} for the parent phase to martensite transformation and A_{max} for the reverse transformation plotted versus temperature. Figures 3 and 4 are the first, second, eighteenth, and one-hundredth cycle peak maximums superimposed for M_{max} and A_{max} respectively for alloy B. Figures 5 and 6 are the respective plots for alloy D. Both alloy samples were as quenched and received 0.0 percent deformation. The major difference between alloy B and alloy D is the M_s temperature. Alloy B has an M_s temperature above ambient and is expected to exist as martensite at room temperature. Alloy D has an M_s which is subambient and is

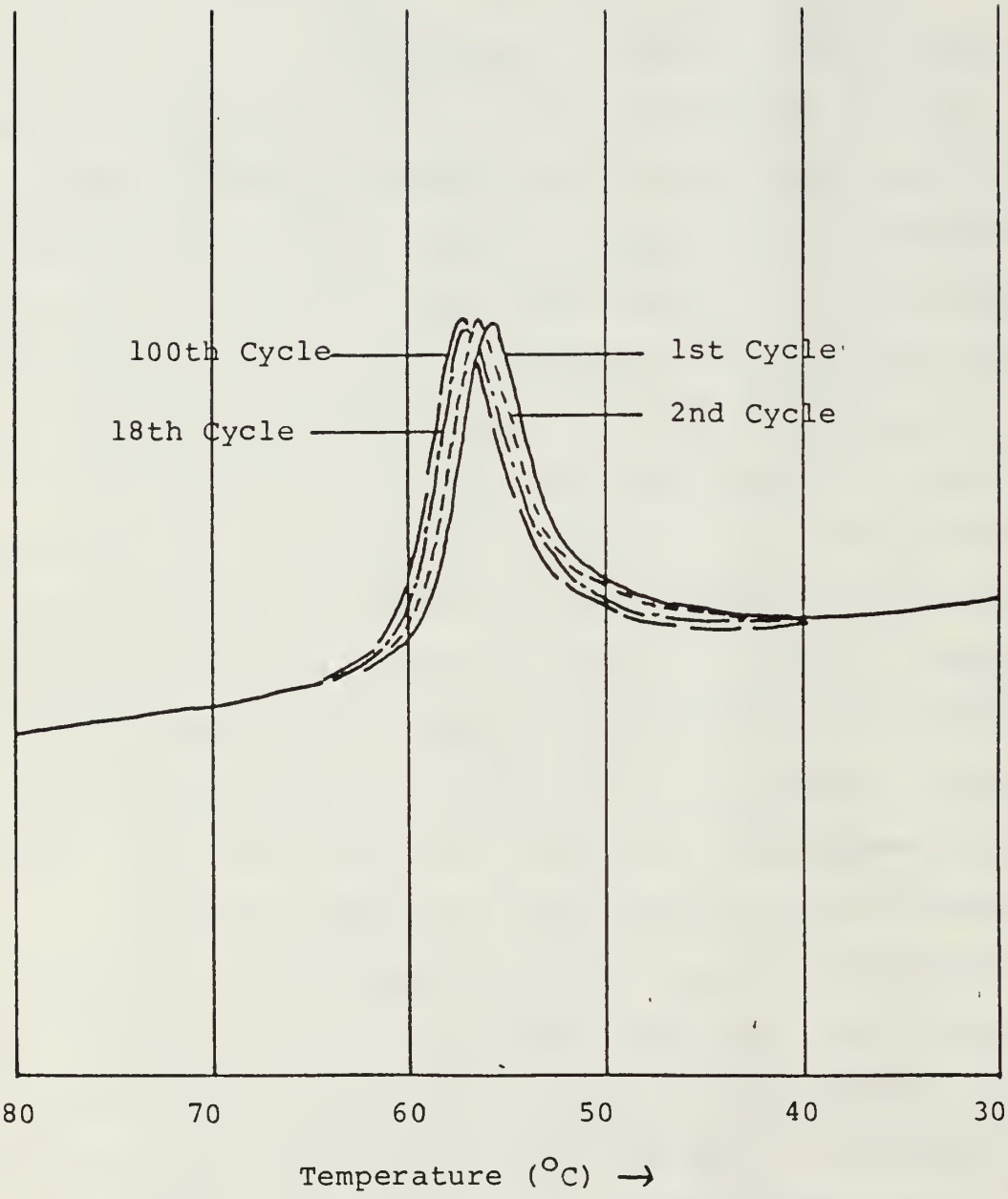

Figure 3. Alloy B, M_{max} Peak Profiles for 1st, 2nd, 18th, and 100th DSC Cycle, 0.00% Cold Work

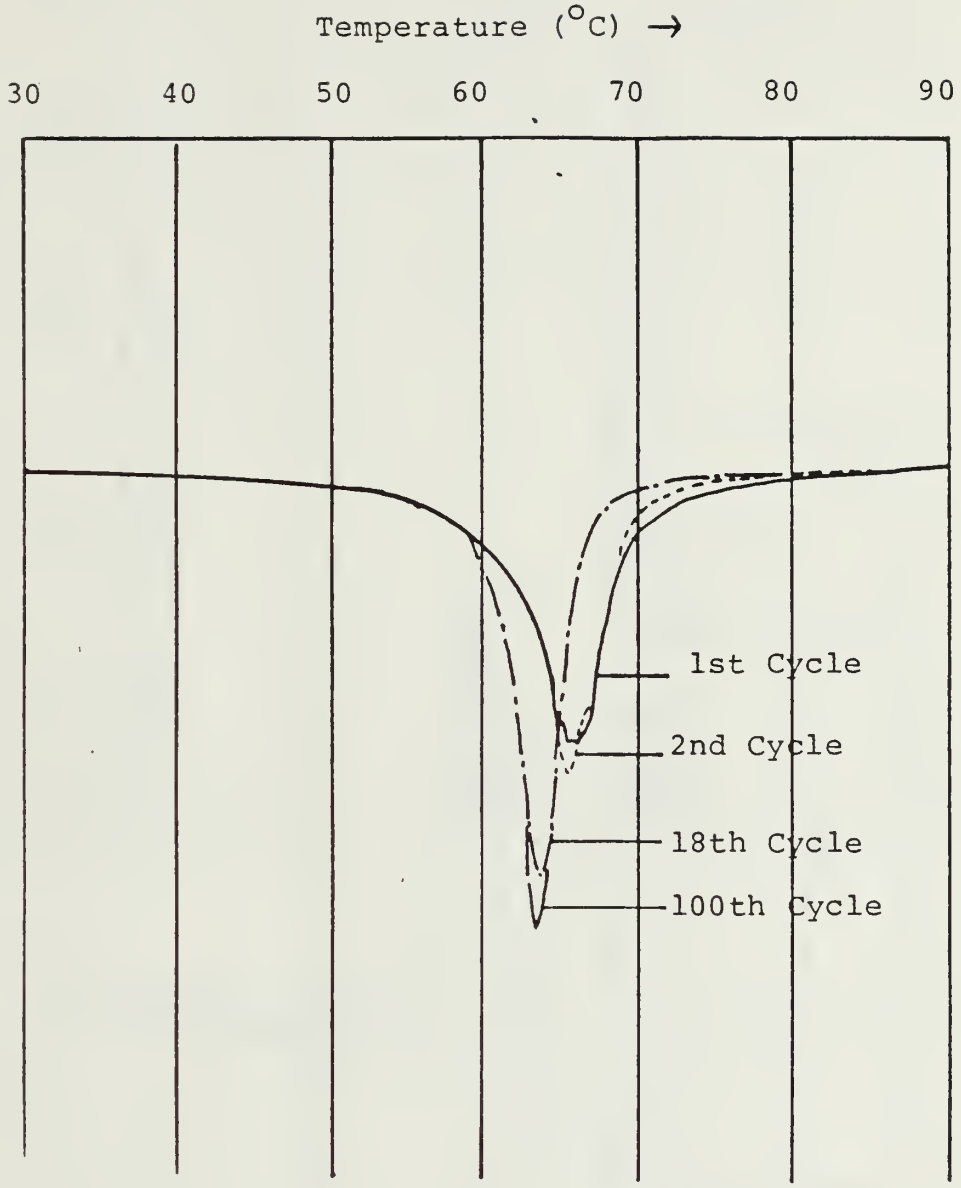

Figurer 4. Alloy B, A_{max} Peak Profiles for 1st, 2nd, 18th, and 100th DSC Cycle, 0.00% Cold Work

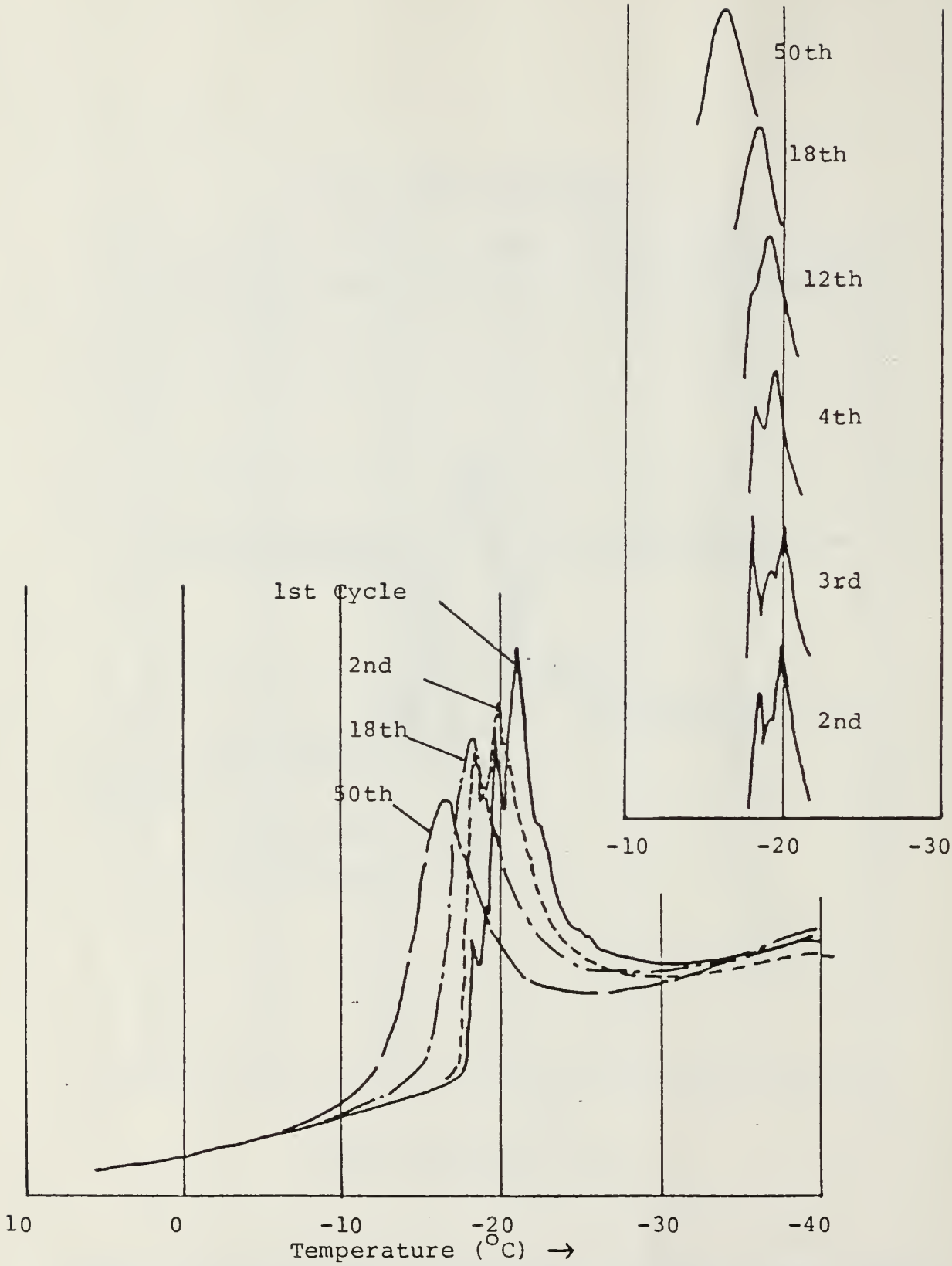

Figure 5. Alloy D, M_{max} Peak Profiles for 1st, 2nd, 3rd, 4th, 12th, 18th, and 50th DSC Cycle, 0.00% Cold Work.

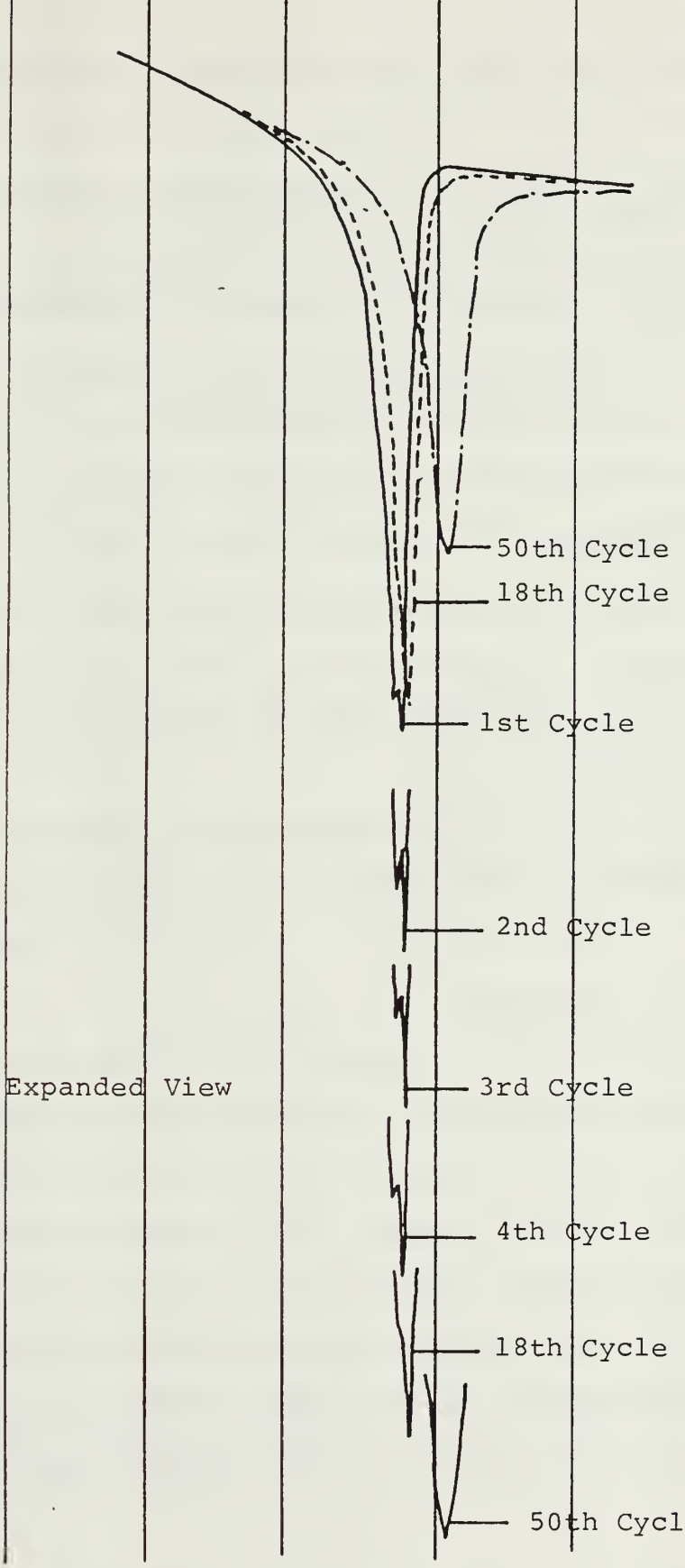

Figure 6. Alloy D, A_{max} Peak Profiles for 1st, 2nd, 3rd, 4th, 18th, and 50th DSC Cycle, 0.00% Cold Work

therefore parent at room temperature. Alloy B displayed the following thermal characteristics:

1) M_{max} gradually increased as A_{max} decreased (i.e., thermal hysteresis decreased).

2) The first few cycles are sporadic but M_{max} and A_{max} stabilize to some value approximately after 15 cycles.

3) M --> P transformation gets more "peaked" (i.e., the width per Figure 2 decreases).

Thermal characteristics of alloy D follow:

1) Both M_{max} and A_{max} increase. Hysteresis decreases slightly.

2) Saturation occurs after approximately 100 cycles.

3) Both P --> M and M --> P peaks get less "peaked". The transformation energy (peak area) approximately remains the same although there is some modest decrease.

4) Fine detail of peaks appear in first several cycles.

These results differ somewhat with results obtained by Perkins and Muesing [Ref. 7] and Boboweic [Ref. 8] which show A_{max} decreasing.

The fine detail of the peaks of alloy D is an interesting phenomenon. Each small peak on the initial cycles is considered to reflect the "burst" (serge as used by Pops and Massalski [Ref. 9]) transformation of martensite plates. Examination of the variation in peak profiles as the cycling is increased reveals that each "burst" formation occurs almost at the same temperature (Figure 5) but gradually merges into one major peak while

the location of the main peak slowly shifts towards higher tempertures as the cycle continues.

There are various obstacles that one might imagine could hinder the continuous growth and expansion of individual martensite plates, such as grain boundaries, dislocations, vacancies, anti-phase boundaries, and precipitates. Some of these obstacles can be rearranged by the cyclic forward/ reverse transformation. According to the Ostuka-Wayman model [Ref. 10] the process of martensite transformation is the creation of close-packed planes and the expansion of partial dislocation loops. In this view, it is clear to conceive the rectification of the transformation path (or "trail-making" [Ref. 7]) with the increase in cycling since repeating passage of partial dislocations would settle out the inhomogeneous obstacles into more stable positions or configurations.

The gradual increase in M_{max} and decrease in A_{max} (in the case of alloy B) can be explained in the same manner. On cooling, the martensite transformation can start at a higher temperature, i.e., lower chemical driving force if the transformation path is well "paved" by prior cycles of transformation. Similarly, on heating the reverse transformation can start earlier; the amount of overheating beyond the equilibrium temperature T_e to trigger the transformation may be less.

The fine detail in alloy D peaks which is not found in alloy B peaks can also be explained. Martensitic transformation of Cu-Zn based alloys is athermal in general but microscopically the process of partial dislocations overcoming obstacles is a thermally-activated process. Thus the alloy D having transformation temperatures in subambient ranges revealed each "bursting" of martensite group formation, while the transformation process of alloy B having M_s temperature above ambient can more smoothly proceed because it has greater assistance from thermal energies.

The increase in A_{max} in the case of alloy D, however, cannot be explained in terms of "trail-making". This increase in A_{max} means that martensite is more stable with respect to the parent phase. The temperature of the quench after homogenization was in a range where the parent phase of alloy D is stable. The quenched-in vacancies will migrate into dislocations and grain boundaries to form the most stable configuration possible in the parent phase. But these defect arrangements may not be as favorable in the martensite phase, so that the defects may rearrange themselves into more stable positions in the martensite phase as cycling and/or aging continues.

Figures 7 and 8 show the 23rd heating and cooling cycle peaks of alloy D samples cold worked by 0.0%, 2.2%, and

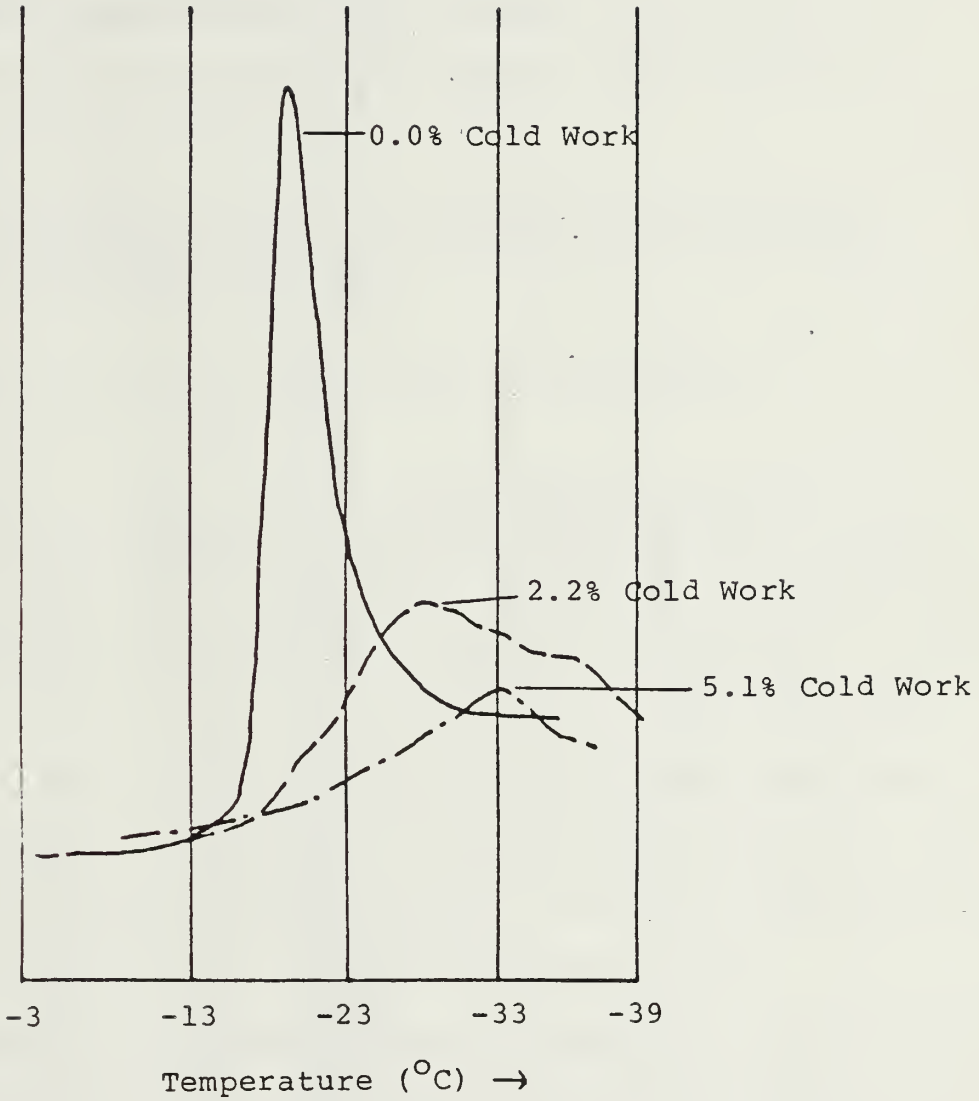

Figure 7. Alloy D, M_{max} Peak Profiles for 23rd DSC Cycle for 0.0, 2.2, 5.1 Percent Cold Work

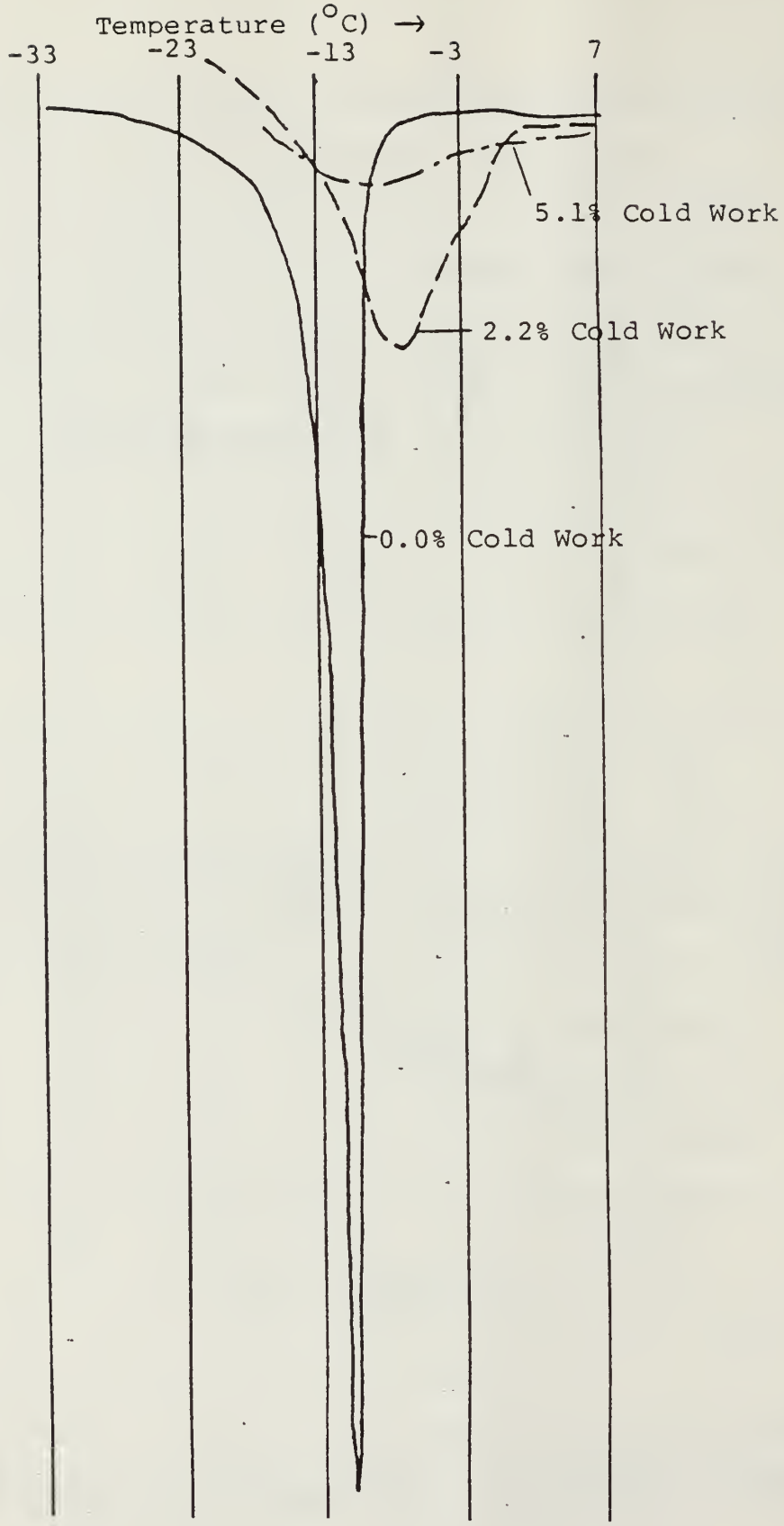

Figure 8. Alloy D, A_{max} Peak Profiles for 23rd DSC Cycle for 0.0, 2.2, 5.1 Percent Cold Work

5.1%. These samples were cycled between 23°C to approximately -94°C by shifting the sample back and forth between absolute methanol at ambient and at or near its freezing point every ten seconds.

The samples were then cycled between 20°C and -50°C. The cold worked alloy D samples displayed the following thermal characteristics:

1) Drastic change in peak height and half-maximum width. As the percent cold work increased the peak height decreased and the width increased as the peak shape became somewhat distorted.

2) Spreading out of peaks (larger hysteresis) and decrease in total area of the peaks as more deformation is applied.

3) Shifting of M_{max} towards lower temperatures and shifting of A_{max} towards higher temperatures with the increase of cold work (with the exception of A_{max} for 5.1% cold worked samples that showed little change).

Decrease in total area of the peak is a direct indication that the amount of martensite transforming back and forth as the temperature is changed to above and below the transformation temperature range has been decreased remarkedly by the applied cold work. As will be shown in the next sections this is directly related to the stabilization of the stress-induced martensites at the light deformation level and to the creation of the α_1' martensite at the heavy deformation level.

The spreading out of the peaks over wider temperature range suggests to us that the smooth thermoelastic

initiation and completion of martensite growth and shrinkage are not the case anymore with the cold worked samples. Martensite plate would not be able to grow large in the forest of stabilized martensite plates.

Generally two opposing effects are expected from the applied cold work; either to assist the martensite transformation by introducing more nucleation site or to interrupt the martensite transformation as the introduced defects act more as the obstacles than as the catalysts. Figures 7 and 8 clearly shows that the latter is the case since the appearance of transformation peaks was retarded on both forward and reverse transformations.

In order to see the stability of the stress-induced martensites introduced by the applid cold work, a short-time heat treatment, at 100°C for 10 minutes, was made for the moderately cold worked (5.1%) specimen. The effect of this short-time heating is shown in the DSC profiles of Figure 9. The peak profiles did not vary much for the first 7 cycles as some of these are shown in Figure 9. However, after heating the specimen up to 100°C and holding it for 10 minutes the next DSC profiles (the 8th cycle) showed clear shifts towards the lower temperatures on both cooling and heating, while the peak size and shape did not change appreciably. This experiment, together with the optical microscopic observations mentioned later on, indicates that

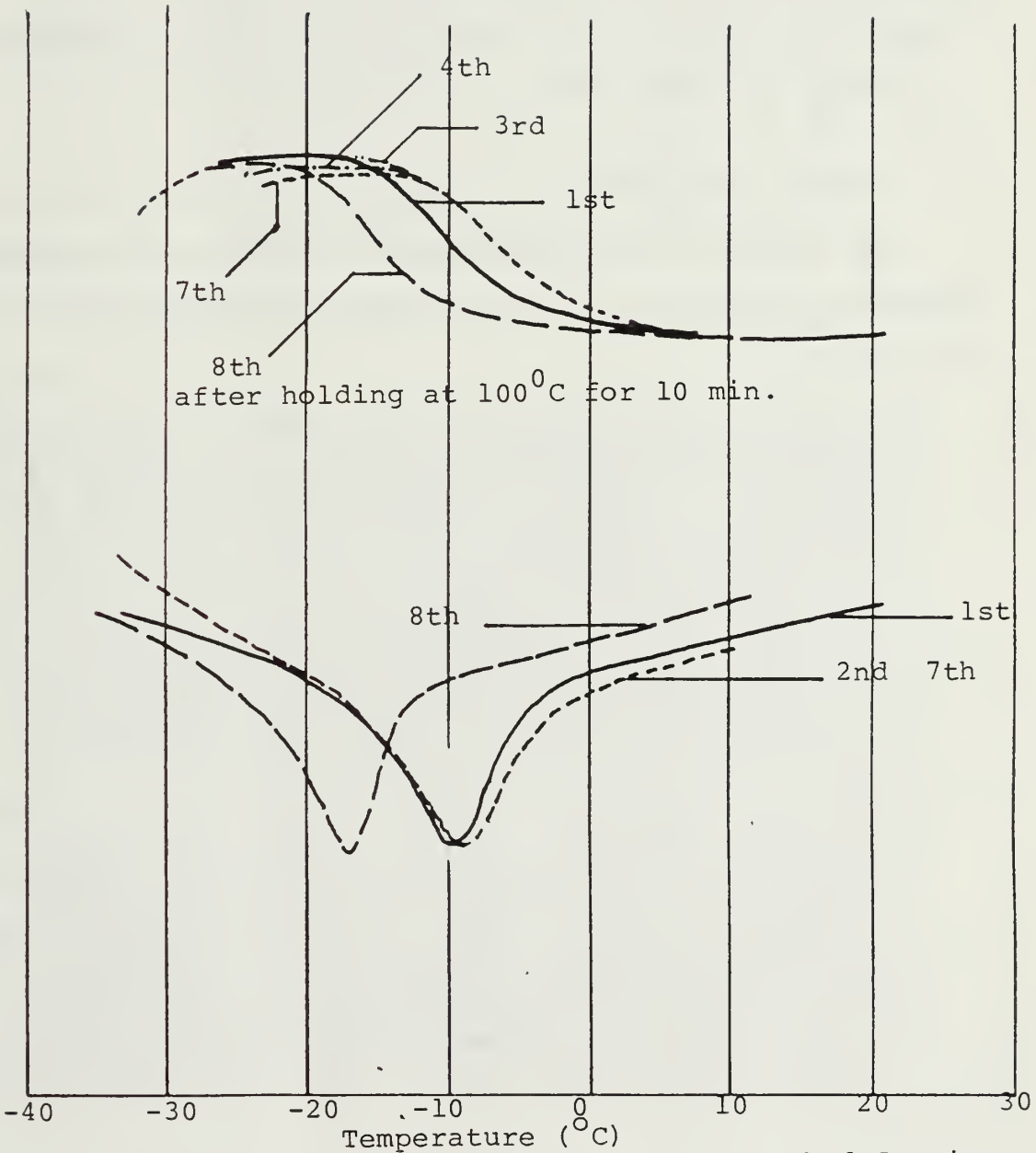

Figure 9. Alloy D, DSC Profiles for 5.1% Cold Worked Specimen Before (1st - 7th) and After (8th) the Short-Time Heat Treatment at 100°C for 10 Minutes.

the stress-induced martensites retained after the cold work remained unchanged by this heat treatment, but that the stability of parent phase increased. The most likely origin of the parent-phase stabilization is conjectured to be the defects related to the quenched-in vacancies that perhaps have taken more stable sites and arrangements upon the short-time heating. This rearrangement also would enhance the state of order.

B. OPTICAL MICROSCOPY

In general, three deformation processes are expected that can contribute to the deformation-induced stabilization of martensite:

1) Variant-Variant Interaction. There are 24 possible variants from a single crystal of β_1. Under uni-axial stress, one favorably-oriented variant grows at the expense of others to become a single crystal of β_1' martensite. Our alloy is a polycrystal and has undergone complex stress by rolling; therefore, complications arise especially along grain boundaries and many variants impinge each other in their growth process. Many combinations of variant impingement for α_1' (3R) martensite at the intersection [Ref. 11], other variant impingement perhaps introduces incoherent interfaces between which are practically irreversible in nature upon unloading.

2) Internal Twinning. Parent β_1 does not deform by twinning since it is easier to deform by forming martensite. In 18R (β_1') martensite, reported twinning planes are [Ref. 12] (128), (128) A:C type interface, (1210), (1210), (1010) A:D type interface, and conjugate twins of all the above (conjugate of (128) is the A:B type interface). Some internal twins can invoke twins in the adjoining variants due to their stress fields at the tips in the direction of their length.

3) Martensite-to-Martensite Transformation. It was observed from X-ray diffraction experiments (will be presented later on) that 9R --> 3R transformation takes place in alloy D. This transformation occurs by shearing on the close-packed plane (009). By similarity of 9R and 3R structures similar internal twinning as mentioned above would occur.

Micrographs 1 through 3 are as quenched samples of alloy D, C, and B respectively. Micrograph 1, alloy D, shows only featureless β_1 with grain boundaries, micrograph 14 is alloy C, which is $\beta_1 + \beta_1'$ at ambient temperature (M_s = 30.8°C, M_f = 18.2°C, A_s = 29.9°C, A_f = 36.0°C at 10th cycle). With the use of polarized microscopy β_1, β_1' phases, and different variants can be differentiated by color. The general features of non-deformed, as quenched fresh thermal martensite are:

1) Straight intervariant boundaries and habit planes,

2) A:B, A:C, A:D combinations,

3) 24 variants divided into 6 plate groups,

4) Many internal striations are either A:D pairs of variants (approximately perpendicular to surrounding intervariant interphases), A:B or A:C pairs (approximately parallel to surrounding boundaries), or internal twins ($\{1210\}_{\beta_1}$, most likely).

Micrograph 3 is alloy B which is completely β_1' at ambient temperature (M_s = 61.1°C, M_f = 44.9°C, A_s = 58.0°C, A_f = 68.8°C at tenth cycle).

Micrographs 4 through 22 are samples of alloy D with various degrees cold work. Basically, since alloy D has an A_f (0.5°C) lower than ambient temperature, the

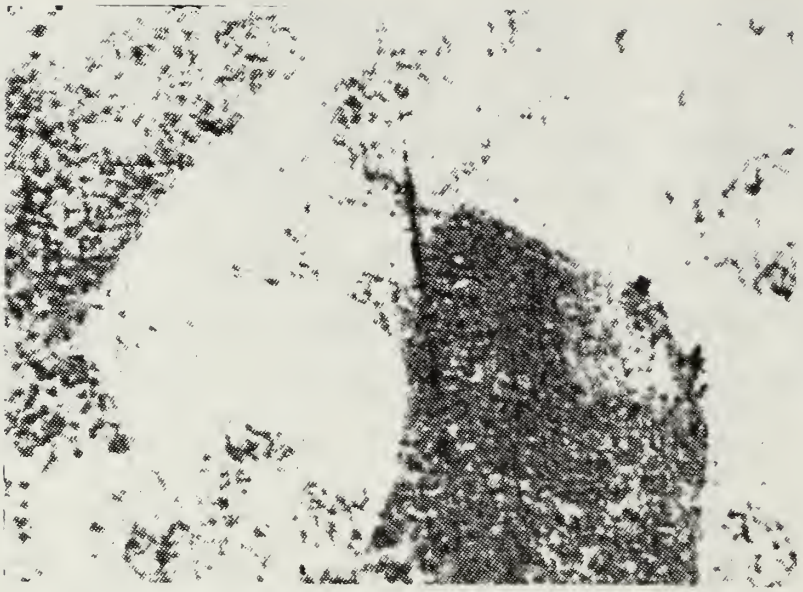

Micrograph 1. Alloy D, 0.00% cold work, parent phase at room temperature, with grain boundaries. (optical, $FeCl_3$ etch, 63X)

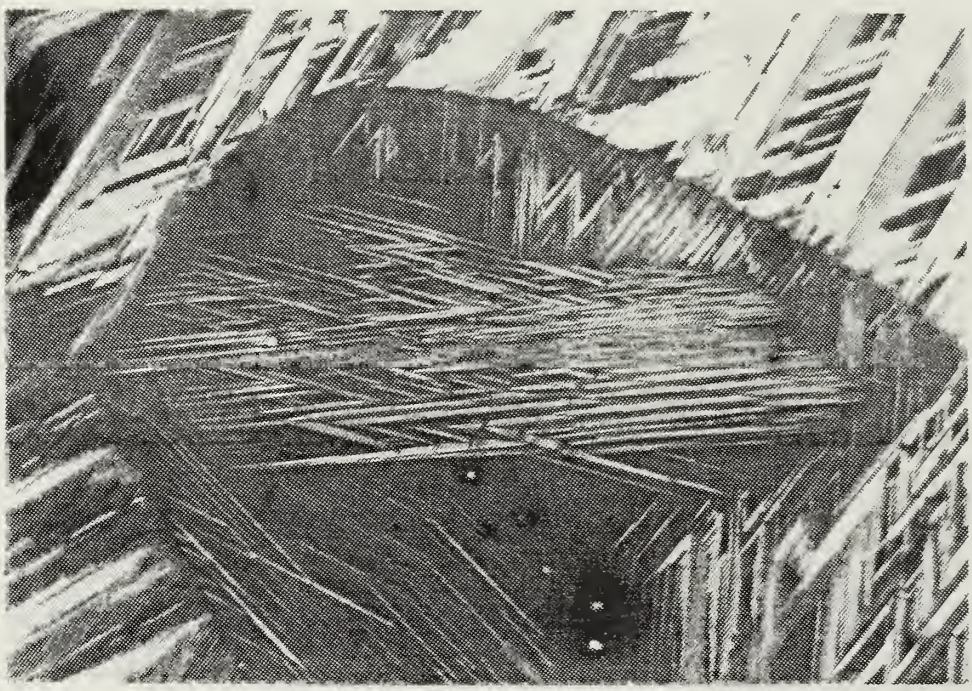

Micrograph 2. Alloy C, $\beta_1 + \beta_1'$ at room temperature. (optical, 63X)

stress-induced martensite (SIM) from cold work should reverse-transform into parent phase upon unloading. However, after unloading many plate-like martensites were retained in all deformed samples.

Micrographs 4 through 7 are samples with 2.2% cold work. Micrograph 4 shows that the linearity of martensite habit plane is not lost. However, many different variants (with angled traces) are seen to intersect or interact at their edges, which could have pinned the martensite, leaving stabilized martensite after unloading. Micrograph 5 shows more stabilized martensite and variant interaction at a higher magnification. The background is β_1 parent. Micrographs 6 and 7 show different characteristic morphologies of variant interactions. Takezawa and Sato [Ref. 11] report that certain combinations of variants crossing produce the α_1' (3R) martensite at the intersection. α_1' does not revert easily back to β_1 and tends to stabilize. These variant combinations have their habit planes angled at close to 90° [Ref. 13]. Micrographs 6 and 7 appear to show these stabilized variants with α_1' at the intersections.

Micrographs 8 and 9 are samples with 6.5 percent cold work. Both micrographs show the same variant crossing regions with more retained martensite. Also note the complication and stress (strain) concentrations along grain

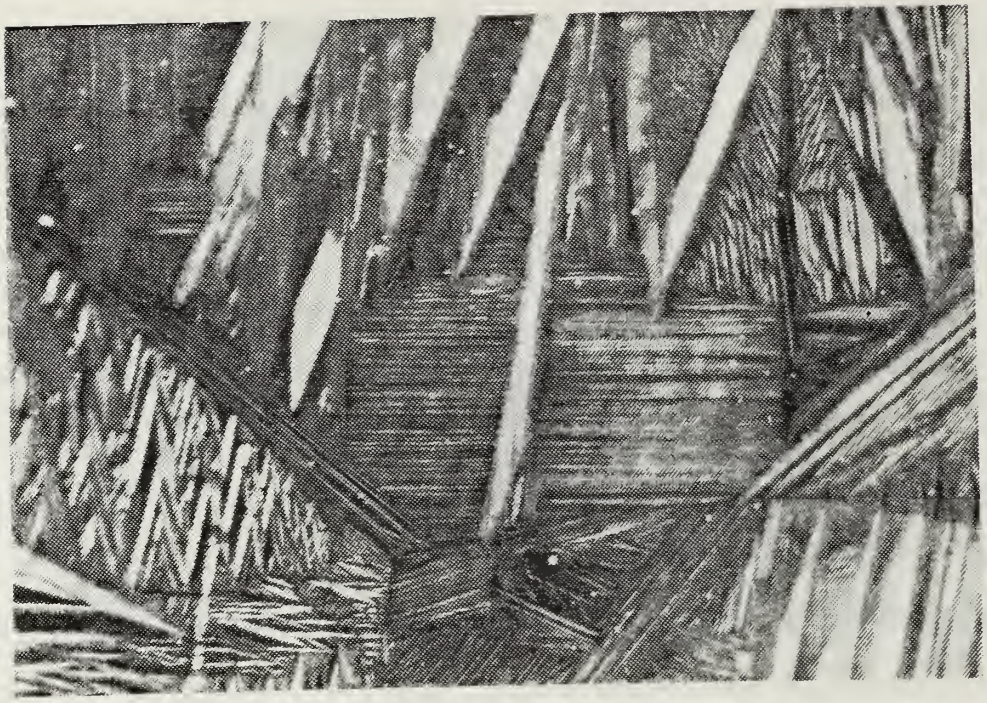

Micrograph 3. Alloy B, completely β_1' at room temperature. (optical, 160X)

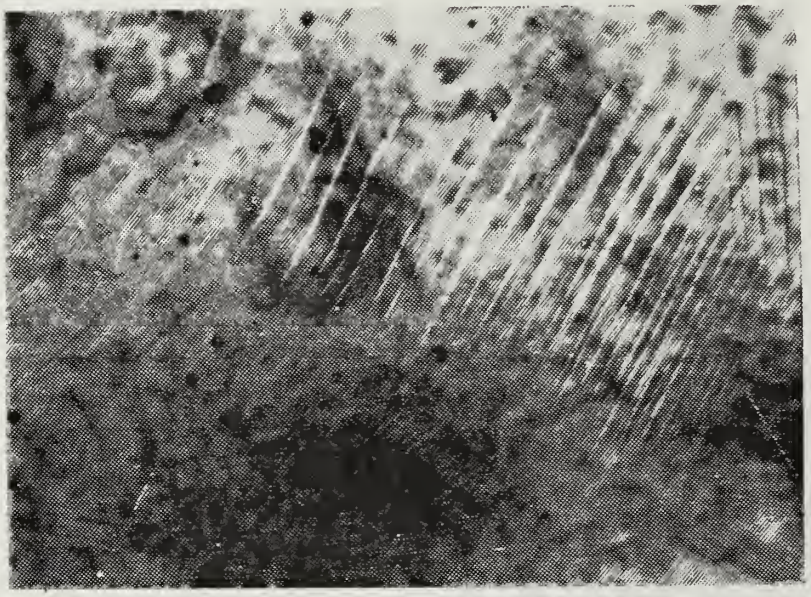

Micrograph 4. Alloy D, 2.2% cold work, stabilized martensite after unloading. (optical, 63X)

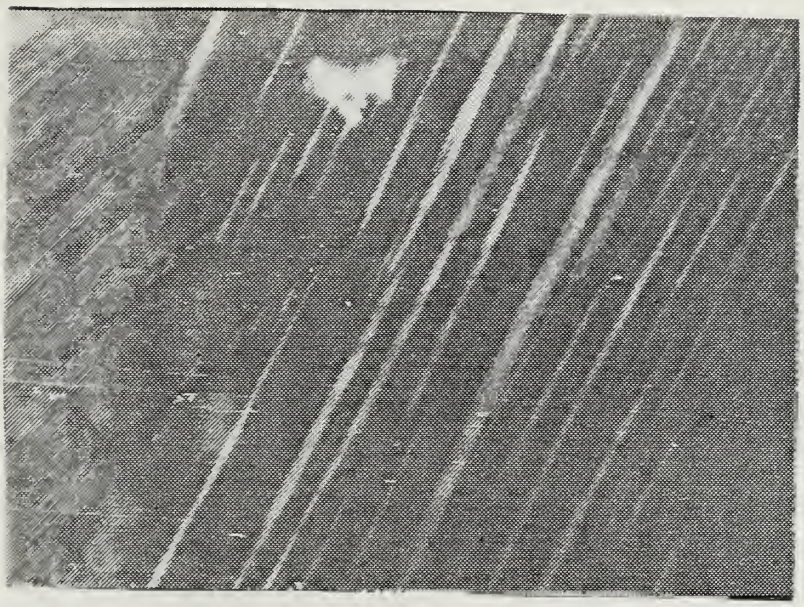

Micrograph 5. Alloy D, 2.2% cold work, stabilized martensite after unloading. (optical, 100X)

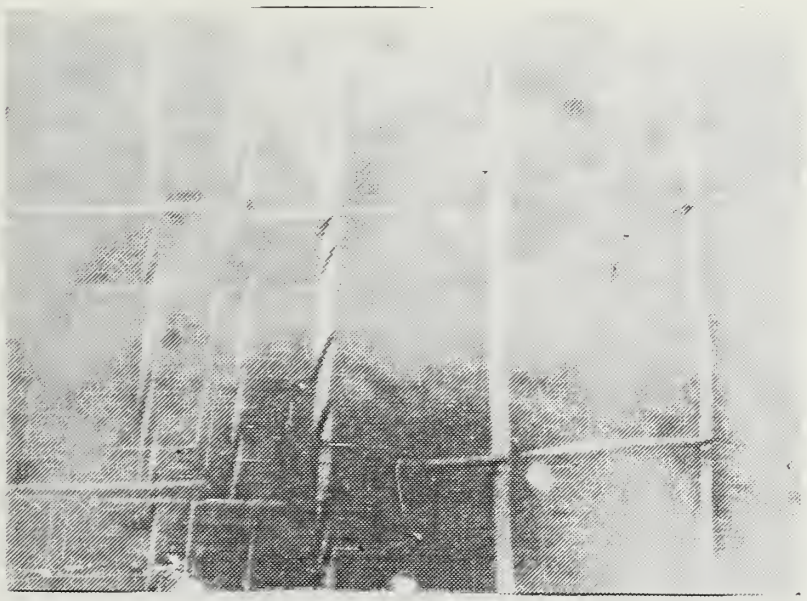

Micrograph 6. Alloy D, 2.2% cold work, martensite variant interaction. (optical, 160X)

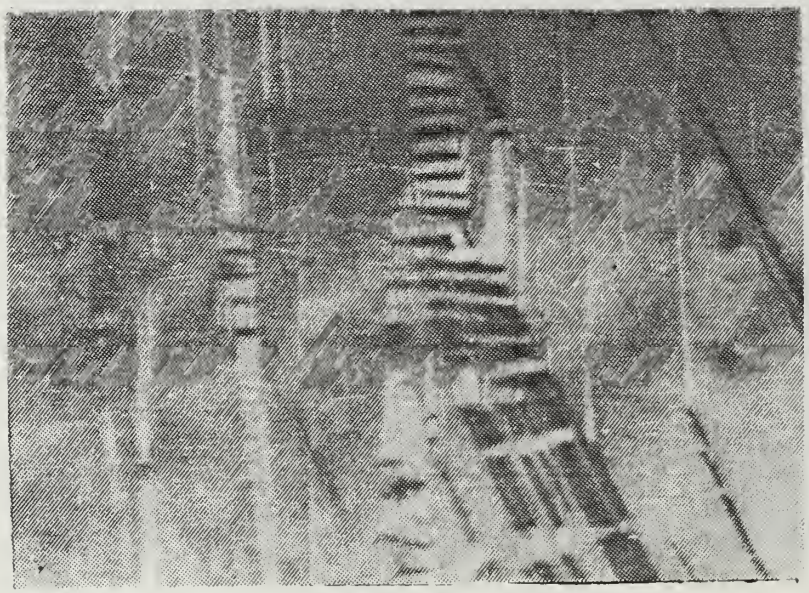

Micrograph 7. Alloy D, 2.2% cold work, martensite variant interaction. (optical, 250X)

Micrograph 8. Alloy D, 6.5% cold work, martensite variant interaction. (optical, 63X)

boundaries of Micrograph 8 where the stress state may have been complex. Micrographs 10 through 13 are samples with 13.9 percent cold work. At this level of deformation an entirely new type of deformation morphology has developed, "wavy structure". In Micrographs 11 and 12, a wavy characteristic of heavily deformed martensite is distinguishable. In general, all four micrographs show much more retained martensite as compared to 2.2 and 6.5 percent cold worked samples. The martensite traces are not always linear but quite frequently curved or kinked. The wavy regions are probably α_1' (3R) judging from the morphological similarity to those observed in cold worked alloy B [Ref. 17]. The internal striations inside the wavy regions of Micrographs 11 and 12 appear to be internal twins in 3R martensite. Micrograph 13 has many regions covered with many martensite traces. Depending on the orientation of the grain, the predominant morphologies occurred from variant interaction and internal twinning.

Micrographs 14 through 17 were cold worked to 18.9 percent. Micrographs 14 and 15 morphologies are equivalent to Micrographs 10 and 11, but the increase of deformation has increased the amount of retained SIM. Micrograph 17 is similar to Figure 3(e) and (f) of Ref. 14. The banded region is stress induced 3R α_1' (habit trace being the basal plane of 18R β_1') and the internally striated region (cross-cross pattern) is basically 9R β_1' with internal

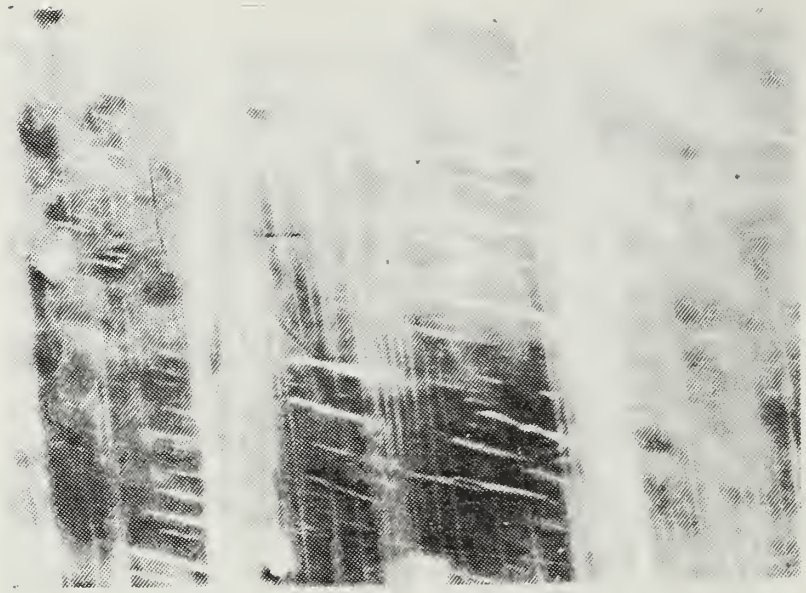

Micrograph 9. Alloy D, 6.5% cold work, martensite variant interaction. (optical, 200X)

Micrograph 10. Alloy D, 13.9% cold work, wavy morphology and internal twinning. (optical, 63X)

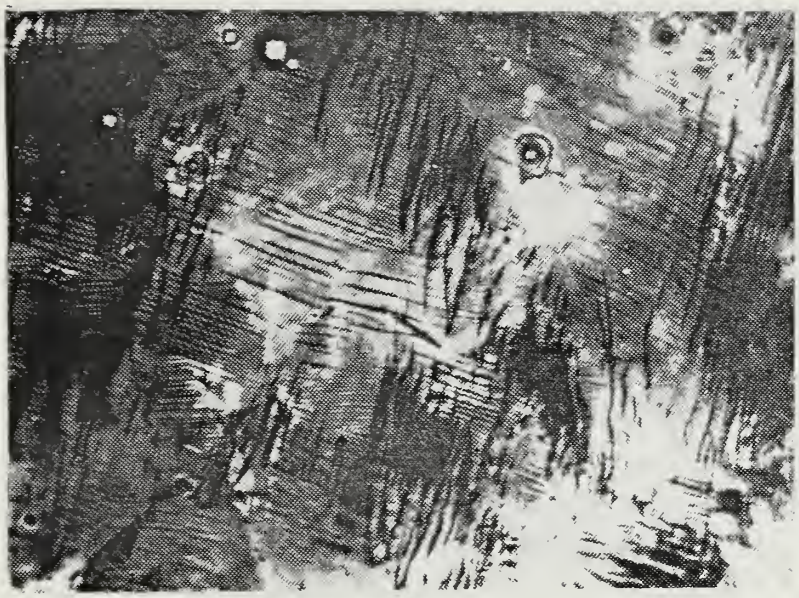

Micrograph 11. Alloy D, 13.9% cold work, wavy morphology and variant interaction. (optical, 63X)

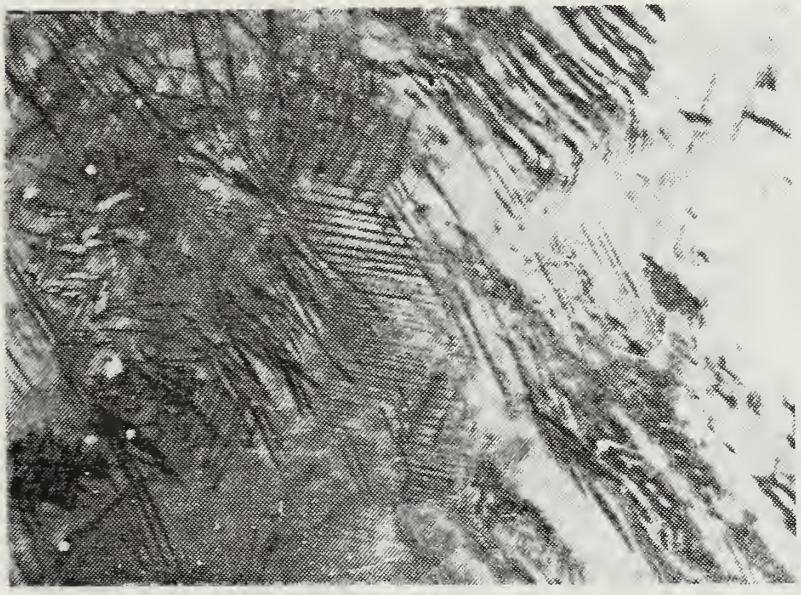

Micrograph 12. Alloy D, 13.9% cold work, wavy morphology. (optical, 63X)

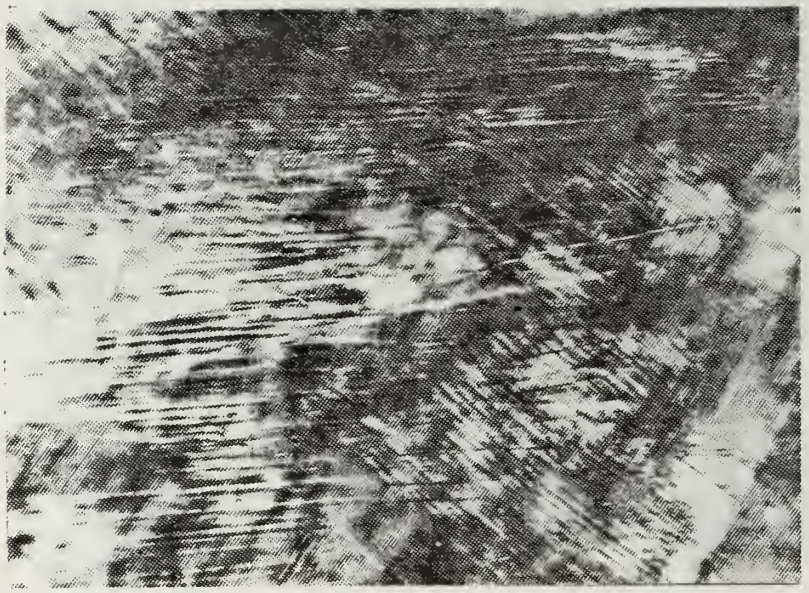

Micrograph 13. Alloy D, 13.9% cold work, wavy morphology and internal twinning. (optical, 63X)

Micrograph 14. Alloy D, 18.6% cold work, wavy morphology. (optical, 63X)

Micrograph 15. Alloy D, 18.6% cold work, wavy morphology. (optical, 63X)

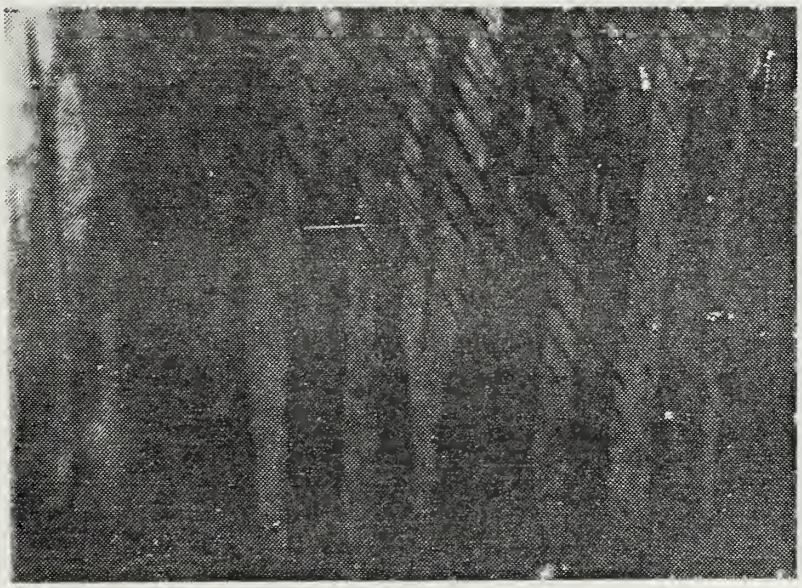

Micrograph 16. Alloy D, 18.6% cold work, internal twinning. (optical, 63X)

Micrograph 17. Alloy D, 18.6% cold work, internal twinning. (optical, 63X)

Micrograph 18. Alloy D, 22.4% cold work, variant-variant interaction and martensite-to-martensite transformation. (optical, 63X)

twins along planes such as $(\bar{1}14)$, $(\bar{1}\bar{1}4)$, (115), $(1\bar{1}5)$, (105) and their conjugate twins. Depending on the kind of variants stacked (black and white bands in Micrograph 16) single twinning (black contrast in Micrograph 16) penetrate the stacked plates.

Micrographs 18 through 22 were cold worked to 22.4 percent. Micrograph 18 has the severest and most complicated morphology but is mainly combinations of variant-to-variant interaction and martensite-to-martensite transformation. Micrograph 19 shows alternating plates deformed in a similar way with an enhanced wavy structure. Micrograph 22 shows the wavy morphology of martensite plates developed in two directions at a much higher magnification. Micrographs 20 and 21 show an interesting morphology in that the deformation of each band introduces rotation, hence the boundary between bands are curved moderately. Additionally, the internal striations (bands) have further banded (Micrograph 21).

Micrographs 23 through 30 show two sets of identical regions of the specimen cold worked by 5.1% before and after the short-time heat treatment of 100^{o}C for 10 minutes. The DSC plots of this sample were already presented in Figure 9. No visible change in microstructures is noticed, which suggests the high stability of martensites introduced by the cold work.

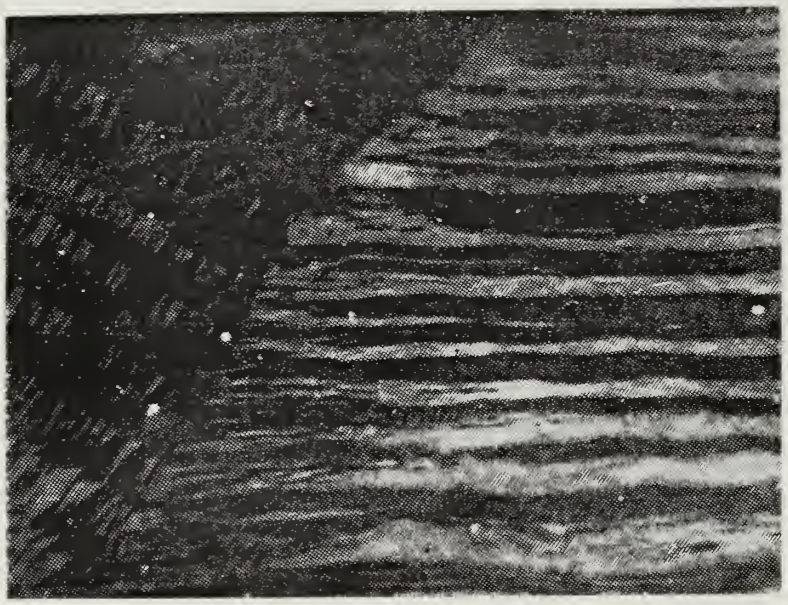

Micrograph 19. Alloy D, 22.4% cold work. (optical, 63X)

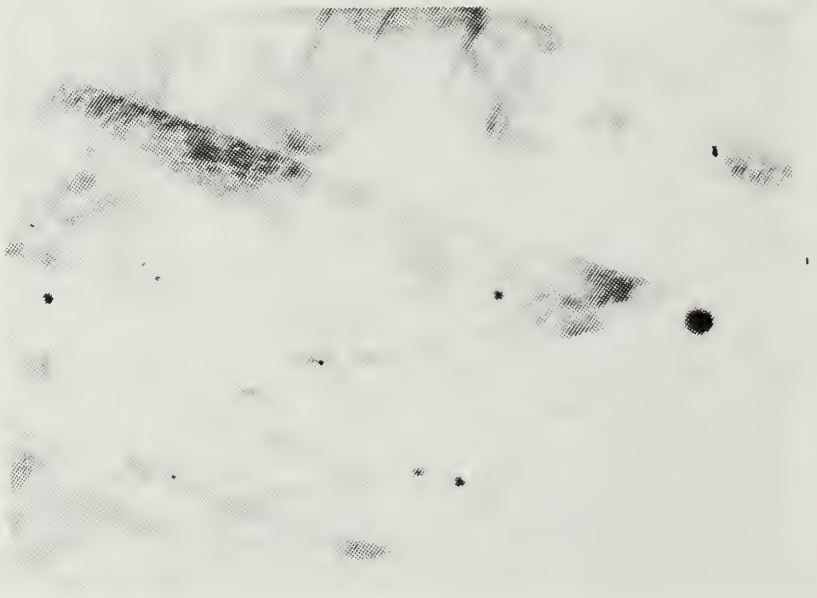

Micrograph 20. Alloy D, 22.4% cold work. (optical, 63X)

Micrograph 21. Alloy D, 22.4% cold work. (optical, 250X)

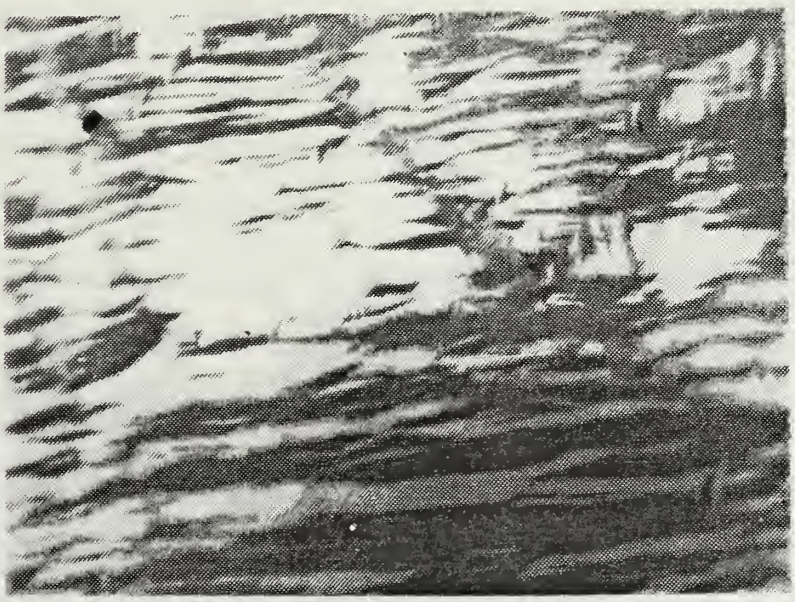

Micrograph 22. Alloy D, 22.4% cold work. (optical, 250X)

C. X-RAY DIFFRACTION

The purpose of the X-ray diffraction study was to obtain information about the structural change due to cold work. Table III summarizes the data obtained.

The structure of the parent phase was analyzed to be the bcc structure. The parent phase is either B2-ordered bcc or

TABLE III

X-RAY DIFFRACTION ANALYSIS RESULTS

ALLOY D

Run	Type of Sample	% Cold Work	Phases Present
1	Bulk	0.0	β_1(B2) + β_1'(9R)
2	Bulk	5.1	β_1 + β_1'
3	Bulk	6.5	β_1 + β_1'
4	Bulk	22.4	β_1 + β_1' + α_1'
5	Powder	0.0	β_1 + α (fcc)
6	Powder	Light	β_1 + α + β_1'
7	Powder	Moderate	β_1 + α + β_1' + α_1'(3R)
8	Powder	Heavy	β_1 + α + β_1' + α_1'

DO_3-ordered bcc. Superlattice reflections do not appear in the present case of Cu-K_α radiation because of the closeness of atomic scattering factors of Cu and Zn. Although the alloy composition is in between the compositions A_3B and AB, we tentatively assumed the order to be B2 because of the relatively small Al content. Therefore, the martensite produced from the parent phase is naturally expected to be

9R, 3R, etc., instead of 18R, 6R, etc. for the case of DO_3 parent. However, the discussion in this thesis will not be altered whether the order is B2 or DO_3. At the end of this section, Table IV lists the calculated reflection angles and Figures 10 through 17 with corresponding Tables V through XII present the x-ray diffraction pattern results.

Analysis of the 0.0% cold work, powder run 5 indicates that the ice-water quench did not prevent the α phase precipitation. Appearance of the α phase in run 5 shows that the decomposition of β into α is relatively easy in this alloy composition. The α phase (having disordered fcc) will not go through the structural transformation and is only expected to produce dislocations and possibly {111} fcc stacking faults under external stress (normal response from fcc metals) contributing to the diffraction pattern line broadening.

Powder run 8 (heavy deformation) confirmed the β_1 --> β_1, (9R) transformation. For predicting the line positions, we assumed that the structure of martensite was modified 9R (M9R) (monoclinic) following Tadaki et. al. [Ref. 15]. Though largely correct, the diffraction peak positions do not precisely match the predicted values, the reason being that stress-induced martensite is expected to contain lots of stacking faults on the basal plane. For precise prediction of peak positions we have to use the extended theory by Kakinoki and Komura [Ref. 16]. But here we

approximated the analysis by determining lattice parameters by using reflections not much affected by stacking faulting, such as 310, 024, 0018, etc.

Both powder and bulk diffraction studies confirmed the 9R --> 3R transformation at a high stress level. No evidence of the 9R --> 2H transformation was obtained (If 2H existed, there should be a major peak, $121_{2H-\gamma_1'}$, in between $114_{\beta_1'}$ and $115_{\beta_1'}$ reflections).

From the determined lattice parameters of α_1', we know that values of a, b, and β are close while c is one-third that of 9R. Of course, this is because the α_1' is stress-induced from β_1, by introducing stacking faults on every third basal plane.

The lines corresponding to α_1' emerged for only the high level of deformation. From metallographical observation, the wavy morphology came into view after approximately 13.1% deformation.

D. TRANSMISSION ELECTRON MICROSCOPY (TEM)

Only preliminary TEM work has been completed in this study. Micrographs 23 and 24 were taken of samples cold worked by extruding with a swaging machine and are 5.86 and 11.26% deformed respectively. Each region with the straight habit corresponds to SIM variant that was stabilized after unloading. Crossing regions have different contrast, indicating the orientation and/or structure of these regions are different.

TABLE IV

CALCULATED REFLECTION ANGLES USING DETERMINED LATTICE PARAMETERS AND ASSUMED MODELS

Planes	$d_{calculated}$	$2\theta_{calc.}$
$11\bar{1}\beta_1'$	2.268	39.73
$201\beta_1'$	2.226	40.52
$009\beta_1'$	2.127	42.50
$11\bar{4}\beta_1'$	2.055	44.06
$204\beta_1'$	2.042	44.35
$115\beta_1'$	1.973	46.00
$20\bar{5}\beta_1'$	1.914	47.52
$20\bar{8}\beta_1'$	1.617	56.95
$11\bar{1}0\beta_1'$	1.460	63.72
$2010\beta_1'$	1.470	63.28
$1111\beta_1'$	1.392	67.24
$020\beta_1'$	1.331	70.79
$310\beta_1'$	1.301	72.70
$11\bar{1}3\beta_1'$	1.232	77.45
$1114\beta_1'$	1.179	81.64
$029\beta_1'$	1.128	86.19
$319\beta_1'$	1.119	87.11
$31\bar{9}\beta_1'$	1.101	88.91
$0018\beta_1'$	1.064	92.90
$110\beta_1$	2.0763	43.59
$200\beta_1$	1.468	63.35
$112\beta_1$	1.199	80.05
$220\beta_1$	1.038	95.90
111α	2.129	42.47
200α	1.843	49.44
220α	1.303	72.52
311α	1.112	87.82
222α	1.064	92.83

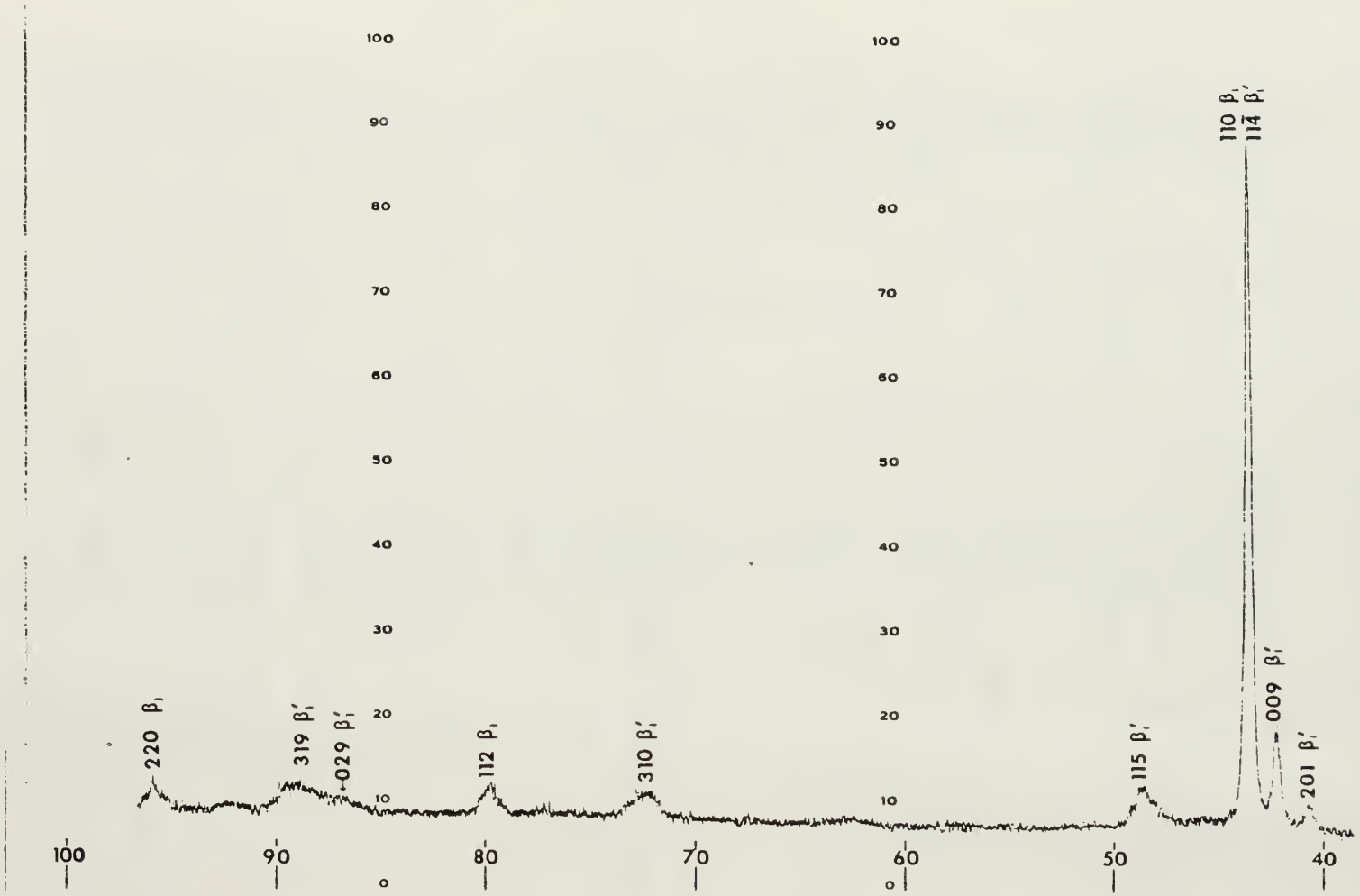

Figure 10. X-Ray Diffraction Pattern Run 1, 0.0% Cold Work, Alloy D, Bulk Sample

TABLE V

TABULATED X-RAY DIFFRACTION PATTERN RESULTS, RUN 1, ALLOY D, BULK SAMPLE, 0.0% COLD WORK

2θ	β_1 (B2)	β_1' (9R)
40.7	--	201
42.2	--	009
43.5	110	$11\bar{4}$
48.6	--	115
72.5	--	310
79.8	112	--
86.8	--	029
88.9	--	319
95.9	220	--

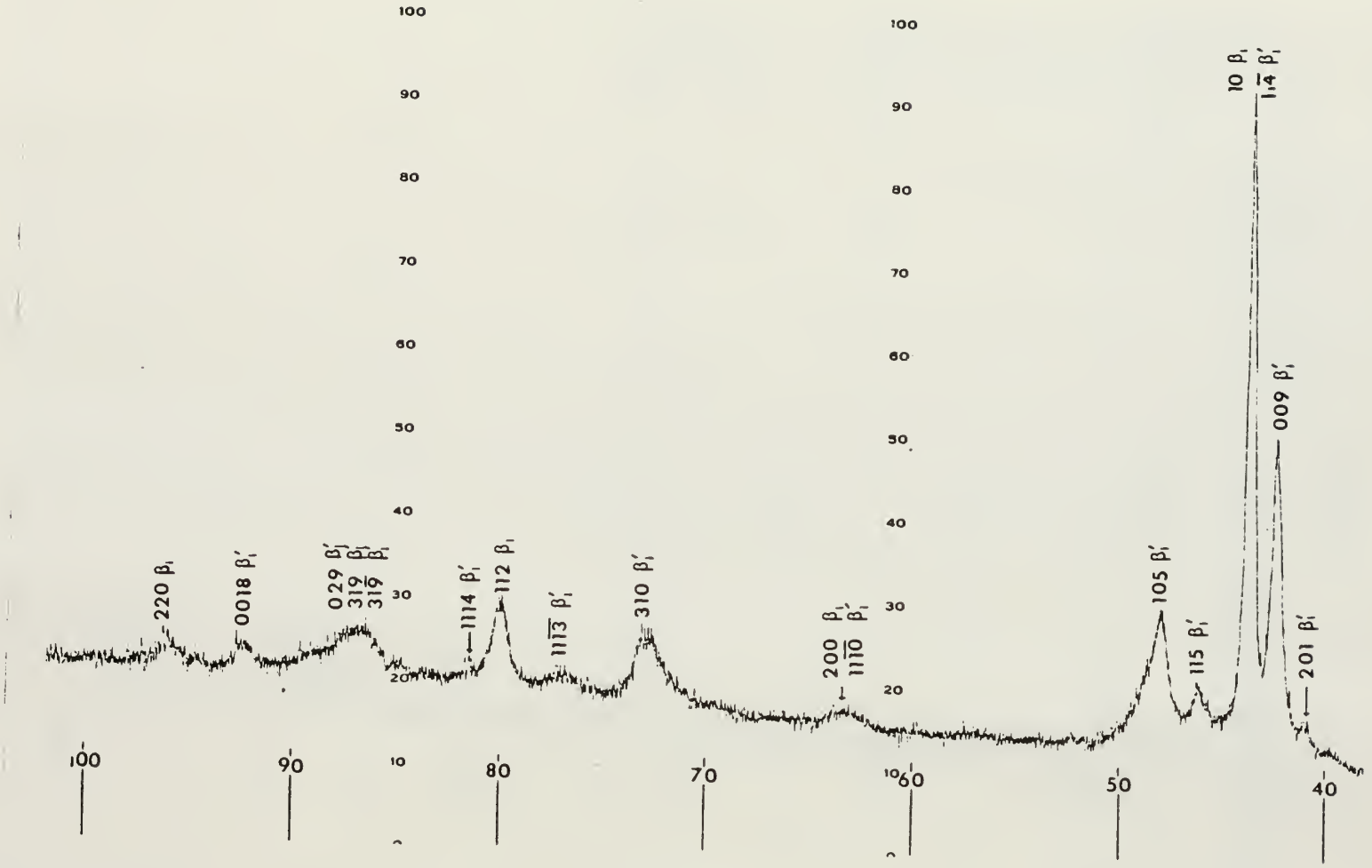

Figure 11. X-Ray Diffraction Pattern Run 2, 5.1% Cold Work, Alloy D, Bulk Sample

TABLE VI

TABULATED X-RAY DIFFRACTION PATTERN RESULTS, RUN 2, ALLOY D, BULK SAMPLE, 5.1% COLD WORK

2θ	β_1 (B2)	β_1' (9R)
41.0	--	201
42.5	--	009
43.7	110	$11\bar{4}$
46.4	--	115
48.3	--	$10\bar{5}$
63.3	200	$11\bar{1}0$
72.8	--	310
77.1	--	$11\bar{1}3$
80.0	112	--
81.4	--	1114
86.8	--	029, 319, $31\bar{9}$
92.5	--	0018
96.1	220	--

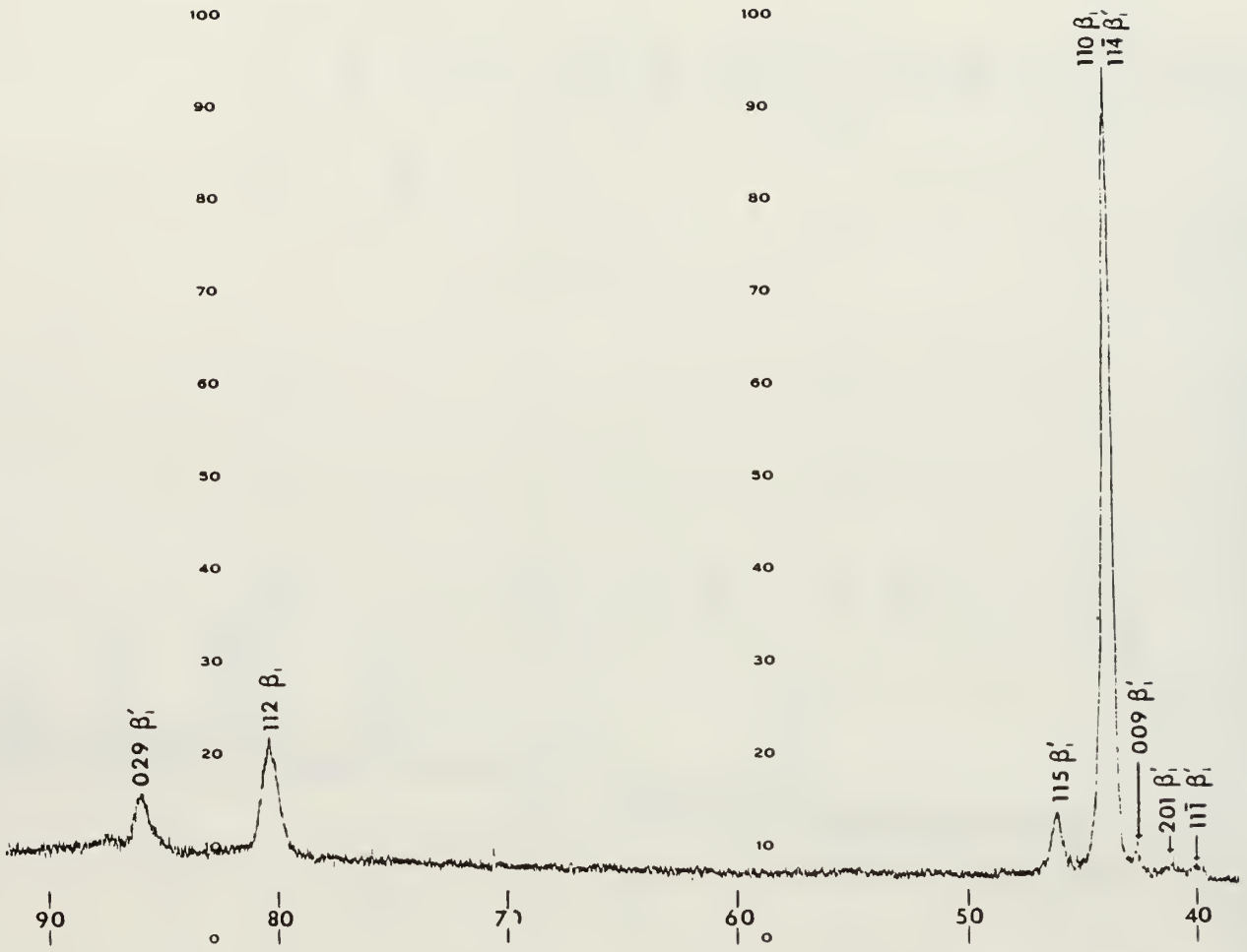

Figure 12. X-Ray Diffraction Pattern Run 3, 6.5% Cold Work, Alloy D, Bulk Sample

TABLE VII

TABULATED X-RAY DIFFRACTION PATTERN RESULTS, RUN 3, ALLOY D, BULK SAMPLE, 6.5% COLD WORK

2θ	β_1 (B2)	β_1' (9R)
40.0	--	$11\bar{1}$
41.1	--	201
42.6	--	009
43.8	110	$11\bar{4}$
46.2	--	$11\bar{5}$
80.5	112	--
86.1	--	029

Figure 13. X-Ray Diffraction Pattern Run 4, 22.4% Cold Work, Alloy D, Bulk Sample

TABLE VIII

TABULATED X-RAY DIFFRACTION PATTERN RESULTS, RUN 4, ALLOY D, BULK SAMPLE, 22.4% COLD WORK

2θ	β_1 (B2)	β_1' (9R)	α_1' (3R)
41	--	201	--
42.5	--	009	003
43.6	110	$11\bar{4}$	--
44.9	--	204	--
46.0	--	115	--
48.2	--	$10\bar{5}$	--
50.8	--	--	112, $20\bar{2}$
63.7	200	$11\bar{1}0$	--
73.2	--	310	310
77.3	--	$11\bar{1}3$	--
80.0	112	--	--
81.7	--	1114	--
86.0	--	029	023
87.6	--	319	313
89.3	--	$31\bar{9}$	$31\bar{3}$
92.7	--	0018	006

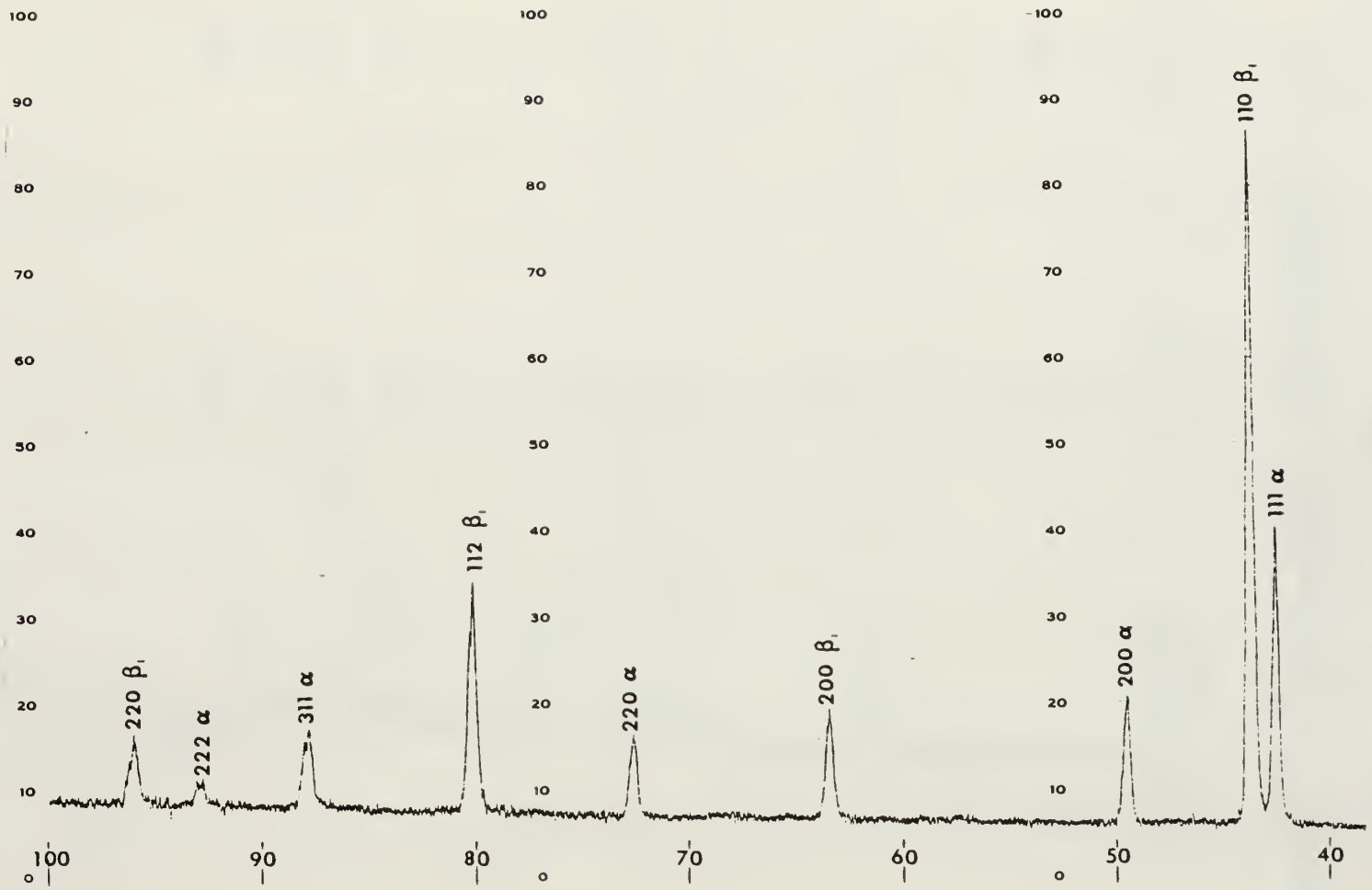

Figure 14. X-Ray Diffraction Pattern Run 5, 0.0% Cold Work, Alloy D, Powder Sample

TABLE IX

TABULATED X-RAY DIFFRACTION PATTERN RESULTS, RUN 5, ALLOY D, POWDER SAMPLE, 0.0% COLD WORK

2θ	β_1 (B2)	α(fcc)
42.4	--	111
43.6	110	--
49.5	--	200
63.4	200	--
72.6	--	220
80.1	112	--
87.8	--	311
92.8	--	222
95.9	220	--

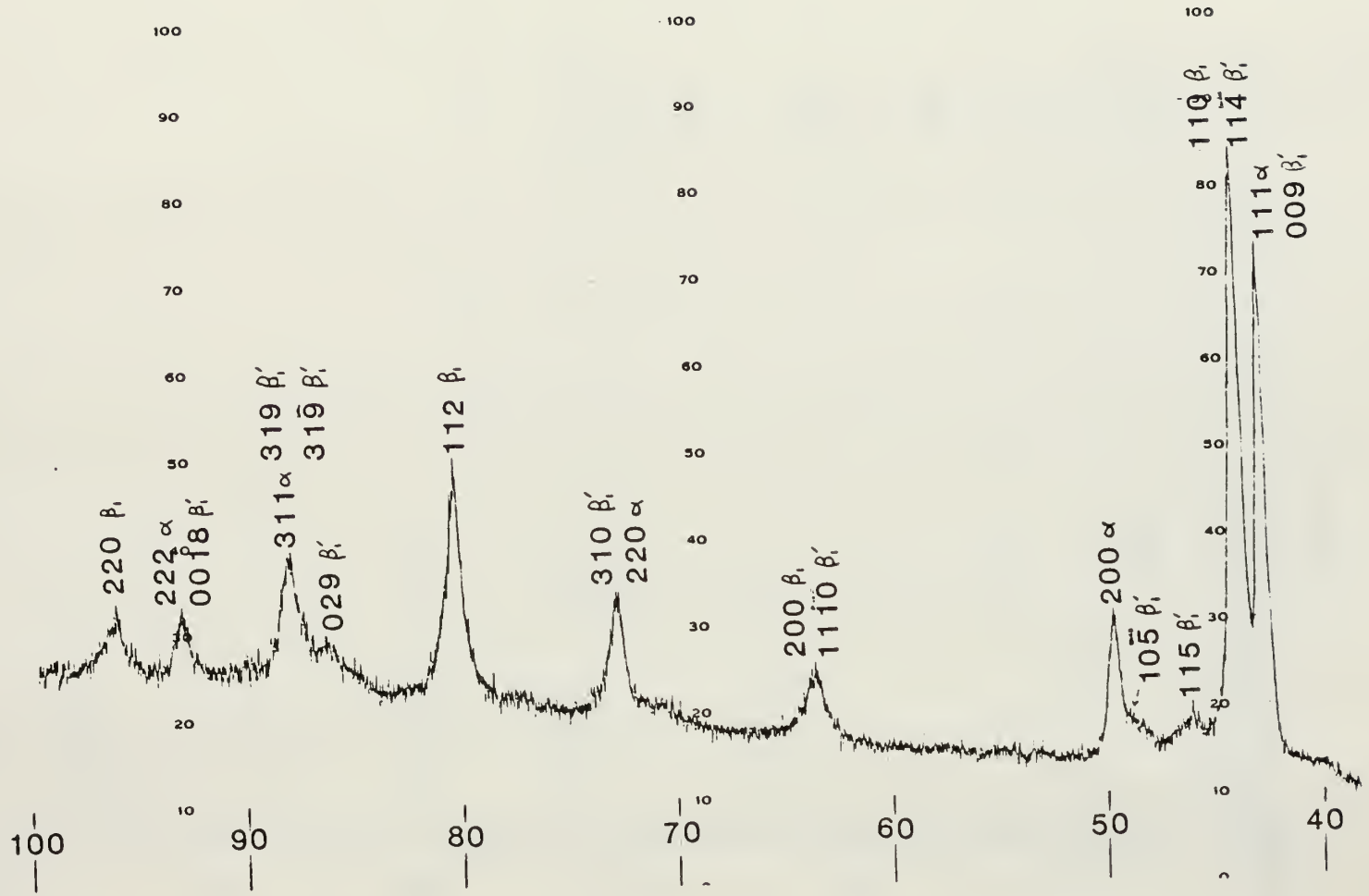

Figure 15. X-Ray Diffraction Pattern Run 6, Light Cold Work, Alloy D, Powder Sample

TABLE X

TABULATED X-RAY DIFFRACTION PATTERN RESULTS, RUN 6, ALLOY D, POWDER SAMPLE, LIGHT COLD WORK

2θ	β_1 (B2)	α (fcc)	β_1' (9R)
42.7	--	111	009
43.8	110	--	$11\bar{4}$
46.0	--	--	115
48.9	--	--	$10\bar{5}$
50.1	--	200	--
63.5	200	--	$11\bar{1}\bar{0}$
72.7	--	220	310
80.2	112	--	--
86.2	--	--	029
87.9	--	311	319, $31\bar{9}$
92.9	--	222	0018
96.0	220	--	--

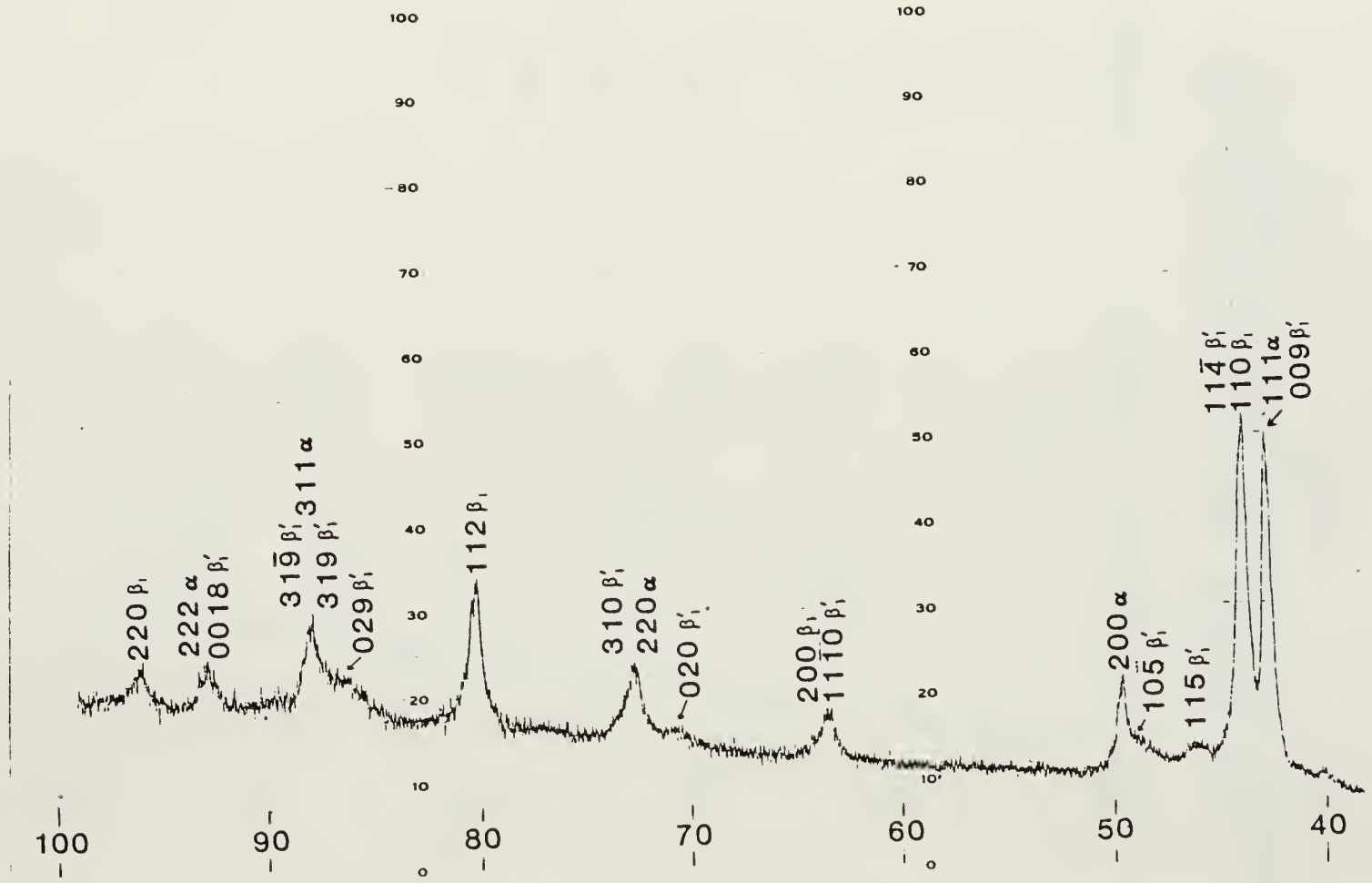

Figure 16. X-Ray Diffraction Pattern Run 7, Moderate Cold Work, Alloy D, Powder Sample

TABLE XI

TABULATED X-RAY DIFFRACTION PATTERN RESULTS, RUN 7, ALLOY D, POWDER SAMPLE, MODERATE COLD WORK

2θ	β_1 (B2)	α (fcc)	β_1' (9R)
40.2	--	--	--
42.7	--	111	009
43.2	110	--	$11\bar{4}$
46.2	--	--	115
48.9	--	--	$10\bar{5}$
49.5	--	200	--
63.5	200	--	$11\bar{1}\bar{0}$
70.8	--	--	020
72.7	--	220	310
80.1	112	--	--
86.2	--	--	029
87.8	--	311	319, $31\bar{9}$
92.8	--	222	0018
95.9	220	--	--

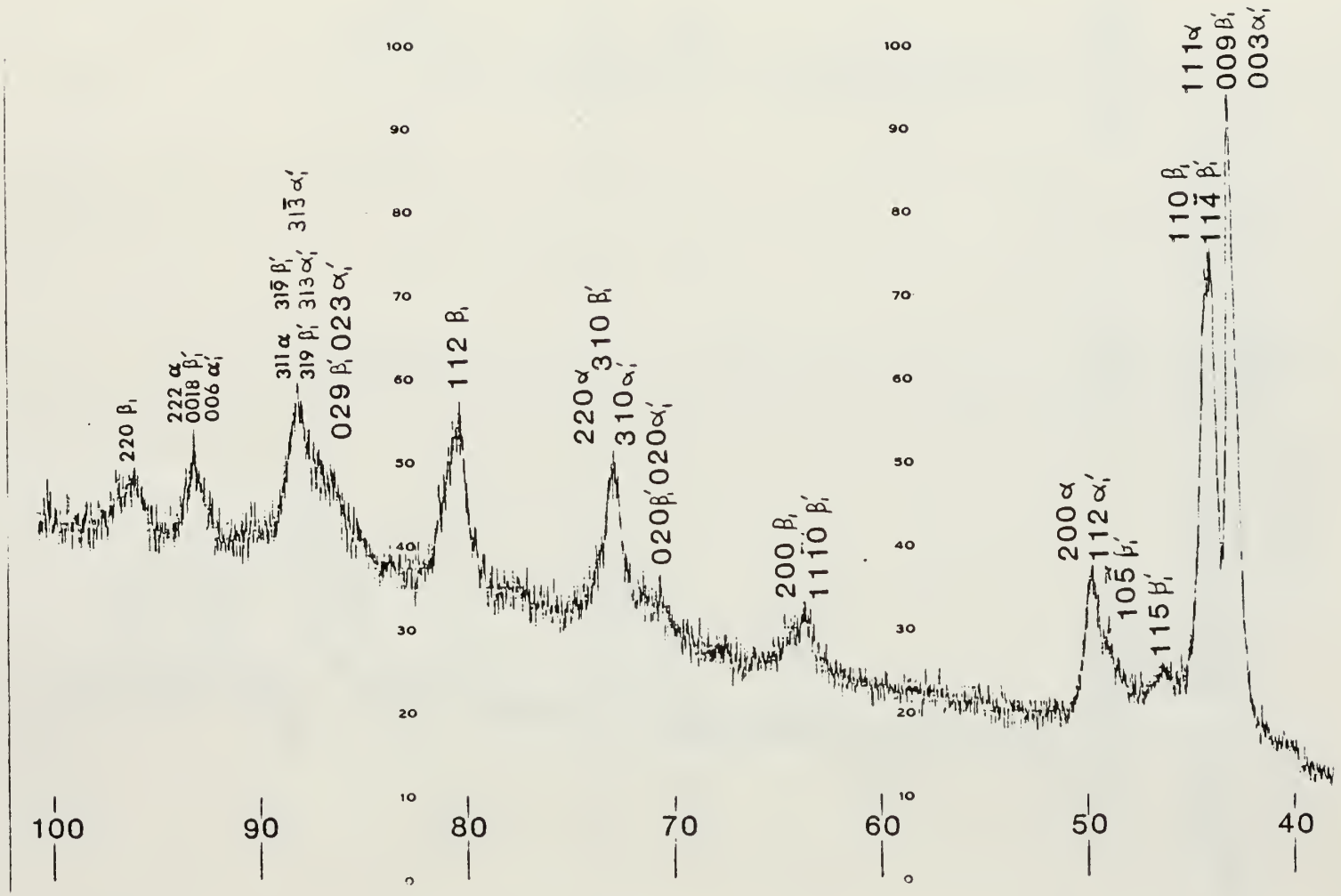

Figure 17. X-Ray Diffraction Pattern Run 8, Heavy Cold Work, Alloy D, Powder Sample

TABLE XII

TABULATED X-RAY DIFFRACTION PATTERN RESULTS, RUN 8, ALLOY D, POWDER SAMPLE, HEAVY COLD WORK

2θ	β_1 (B2)	α (fcc)	β_1' (9R)	α_1' (3R)
40.4	--	--	--	--
42.9	--	111	009	003
43.8	110	--	$11\bar{4}$	--
46.4	--	--	115	--
48.9	--	--	$10\bar{5}$	--
49.7	--	200	--	112
63.6	200	--	$11\bar{1}0$	--
70.6	--	--	020	020
72.8	--	220	310	310
80.2	112	--	--	--
86.4	--	--	029	023
88.0	--	311	319, $31\bar{9}$	313, $31\bar{3}$
93.1	--	222	0018	006
96.2	220	--	--	--

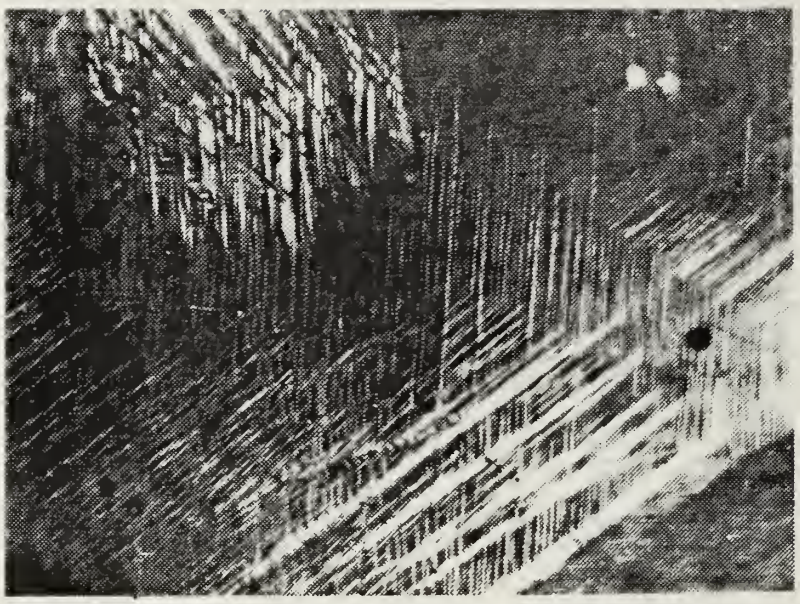

Micrograph 23. Alloy D, 5.1% cold work, 0 thermal cycles. (optical, 63X)

Micrograph 24. Alloy D, 5.1% cold work, 0 thermal cycles. (optical, 63X)

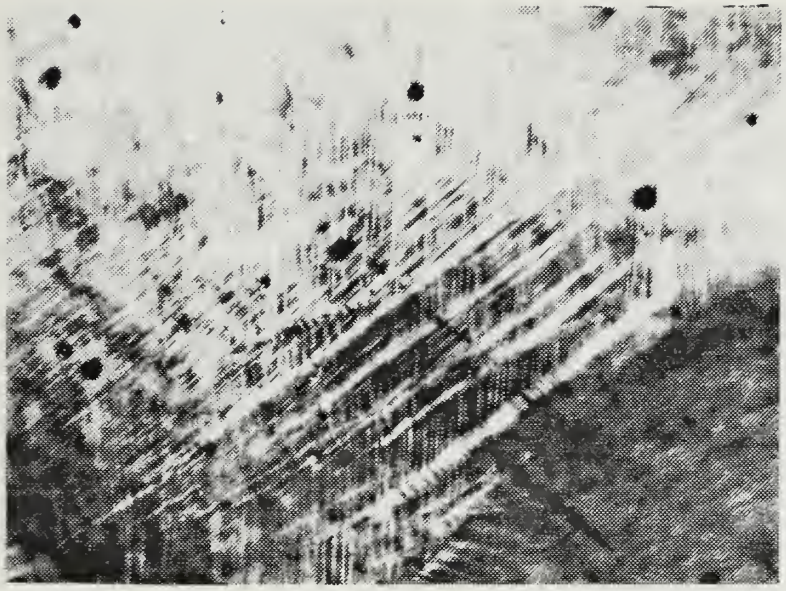

Micrograph 25. Alloy D, 5.1% cold work, after one thermal cycle. (optical, 63X)

Micrograph 26. Alloy D, 5.1% cold work, after one thermal cycle. (optical, 63X)

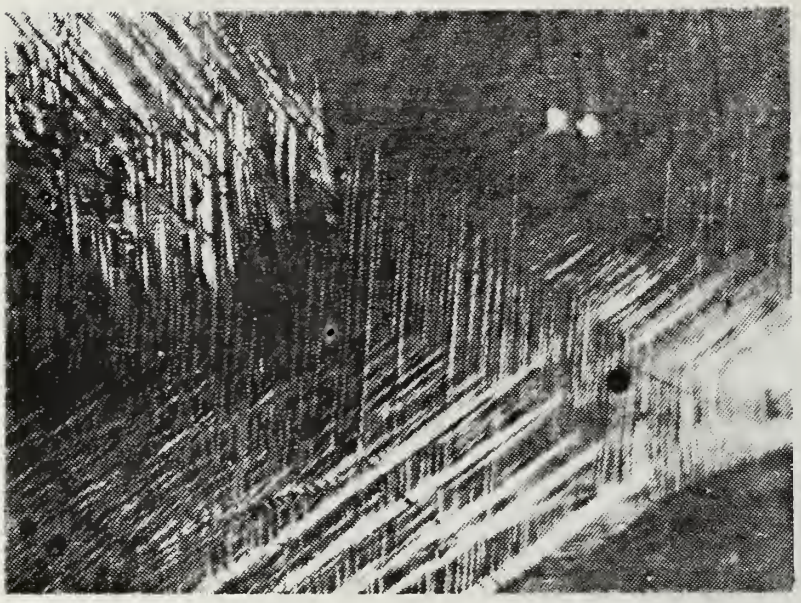

Micrograph 27. Alloy D, 5.1% cold work, after seven thermal cycles. (optical, 63X)

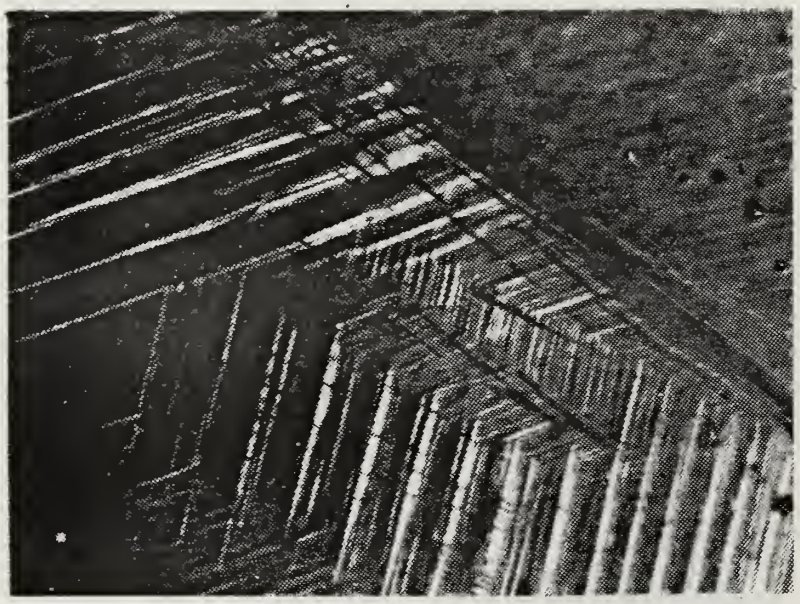

Micrograph 28. Alloy D, 5.1% cold work, after seven thermal cycles. (optical, 63X)

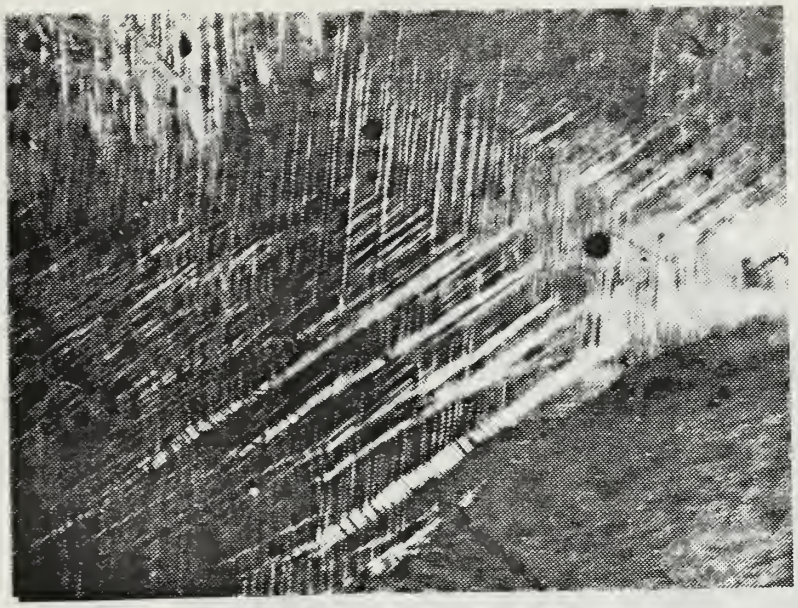

Micrograph 29. Alloy D, 5.1% cold work, after nine thermal cycles. Heat treated for 10 minutes at 373 K after seventh thermal cycle. (optical, 63X)

Micrograph 30. Alloy D, 5.1% cold work, after nine thermal cycles. Heat treated for 10 minutes at 373 K after seventh thermal cycle. (optical, 63X)

Micrograph 31. Stabilized SIM variants, alloy D, 5.86% cold work (TEM 27,000X)

Micrograph 32. Stabilized SIM variants with indications of wavy morphology, alloy D, 11.26% cold work (TEM 14,000X)

VI. CONCLUSIONS

1. The characteristic martensitic transformation temperatures M_{max} and A_{max} gradually increase and decrease respectively during transformation cycling, but stabilize after approximately 15 cycles, in the case of alloy B. A moderate increase of A_{max}, however, was observed for the alloy D, and the number of cycles to a stabilized value was about 100.

2. The "burst" creation of groups of martensite was monitored through the appearance of fine details of DSC profiles for the alloy D, which gradually disappeared after ≈ 15 cycles.

3. Differences between alloy B and alloy D are attributed to the difference in transformation temperatures, i.e., different distribution of quenched-in vacancies and related defects.

4. Cold work at $T > A_f$ stabilized the stress-induced martensite through mutual interaction between martensite variants. This pinning of martensites in the parent phase seems relatively strong and could not be relieved by heat-treatment at 100°C for 10 minutes. Together with a prevailing appearance of crossing morphologies of martensite in these samples, the formation of α_1' martensite at the intersection is the proposed reason for the stabilization.

5. At higher levels of applied stress, a 9R (18R) --> 3R (6R) transition was confirmed by powder x-ray diffraction experiments. The "wavy" morphology is presumably representing this martensite-to-martensite transformation, which was predominant in specimens cold worked by more than 13.6%.

LIST OF REFERENCES

1. Perkins, J., "Shape Memory Behavior and Thermoelastic Martensite Transformations," Mater. Sci. and Eng., v. 51, pp. 181-192, 1981.

2. Shewman, P.G., Transformations in Metals, pp. 323-326, McGraw-Hill, 1969.

3. Nishiyama, Z., Martensitic Transformation, pp. 11-13, 276-277, Academic Press, 1978.

4. Warlimont, H. and Delaey, L., "Martensitic Transformations in Copper-Silver-and Gold-Based Alloys," Progress in Materials Science, v. 18, 1974.

5. Perkins, J. and Sponholz, R.O., "Stress-Induced Martensite Transformation Cycling and Two-Way Shape Memory Training in Cu-Zn-Al Alloys," Met. Trans., v. 15A, pp. 313-321, 1984.

6. Cohen, M. and Wayman, C.M., "Fundamentals of Martensitic Reactions," Reprint: Metallaurgical Treatises, pp. 445-446, 1980.

7. Perkins, J. and Muesing, W.E., "Martensitic Transformation Cycling Effects in Cu-Zn-Al Shape Memory Alloys," Met. Trans., v. 14A, pp. 33-36, 1985.

8. Bobowiec, P., Characterization of the Structure and Substructure of Thermally Transformation Cycled Cu-Zn-Al Shape Memory Alloys, M.S. Thesis, Naval Postgraduate School, Monterey, California, 1983.

9. Pops, H. and Massalski, T.D., "Thermoelastic and Burst-Type Martensites in Copper-Zinc Beta-Phase Alloys," Trans. AIME, v. 230, p. 1662, 1964.

10. Otsuka, K. and Wayman, C.M., "On the Shape Memory Effect in Internally Faulted Martensites," Scripta Met., v. 9, p. 1017, 1975.

11. Sato, H., Takezawa, K., and Sato, S., "Mechanical Behavior Associated with the β_1 -> β_1' -> α_1'' Transformation in Cu-Zn-Al Single Crystals," Proc. Joint U.S. Japan Seminar, p. 92-97, Troy, 1979.

12. Saburi, T. and Nenno, S., "The Shape Memory Effect and Related Phenomena," Proc. Int. Conf. on Solid to Solid Phase Transf., AIME, p. 1455, 1982.

13. Adachi, Kenji, "Phase Transformations in Nearly Stoichiometric Nickel-Manganese Alloys," Doctorial Thesis, University of Illinois, 1983.

14. Adachi, K., Sullivan, S., and Perkins, J., "Deformation of Martensite in a Polycrystalline Cu-Zn-Al Alloy," to be published in Met. Trans.

15. Tadaki, T., Tokoro, M., and Shimizu, K., "Thermoelastic Nature and Crystal Structure of the Cu-Zn Martensite Related to the Shape Memory," Trans. Japan Inst. Metals, v. 16, p. 285, 1975.

16. Kakinoki, J., "Diffraction by a One-Dimensionally Disordered Crystal II Close-Packed Structures," Acta Cryst. v. 23, p. 875, 1967.

BIBLIOGRAPHY

Cornelis, I. and Wayman, C.M., "Phase Transformations in Metastable Beta Prime CuZn Alloys - I. Martensitic Transformations," Acta. Met., v. 22, 1974.

Dvorak, J.R. and Rostoker, W., Interpretation of Metallographic Structures, Academic Press, 1965.

Graves, R.H. and Wrighton, H., Practical Microscopical Metallography, 4th ed., Chapman & Hall, Ltd., 1967.

Schroeder, T.A. and Wayman, C.M., "The Two-Way Shape Memory Effect and Other Training Phenomena in Cu-Zn Single Crystals," Scripta Met., v. 11, pp. 225-230, 1977.

Schroeder, T.A. and Wayman, C.M., "The Formation of Martensite and the Mechanism of the Shape Memory Effect in Single Crystals," Acta Met., v. 25, pp. 1375-1391, 1976.

Schroeder, T.A. and Wayman, C.M., "Pseudoelastic Effects in Cu-An Single Crystals," Acta Met., v. 27, pp. 405-417, 1978.

Shewman, P.G., Transformations in Metals, McGraw-Hill Book Company, 1969.

Weinberg, F., Tools and Techniques in Physical Metallurgy, v. 1, Dekker, Inc., 1970.

INITIAL DISTRIBUTION LIST

		No. Copies
1.	Defense Technical Information Center Cameron Station Alexandria, Virginia 22314	2
2.	Library, Code 0142 Naval Postgraduate School Monterey, California 93943	2
3.	Department Chairman, Code 69 Department of Mechanical Engineering Naval Postgraduate School Monterey, California 93943	1
4.	Associate Professor Jeff Perkins, Code 69Ps Department of Mechanical Engineering Naval Postgraduate School Monterey, California 93943	5
5.	LCDR Gary Moore Box 8, SRF FPO Seattle, Washington 98762	1

Thesis
M766 Moore
c.1 The effect of prior parent phase cold work on martensite transformation in Cu-An-Al shape memory alloys.